Energy 278 (2023) 127868

Contents lists available at ScienceDirect

Energy

journal homepage: www.elsevier.com/locate/energy

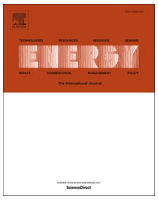

# Process analysis and comparative assessment of advanced thermochemical pathways for e-kerosene production

Konstantinos Atsonios [a], Jun Li [b], Vassilis J. Inglezakis [b,*]

[a] Centre for Research & Technology Hellas, Chemical Process and Energy Resources Institute, 57001, Thessaloniki, Greece
[b] Department of Chemical and Process Engineering, University of Strathclyde, 75 Montrose St., Glasgow, G1 1XJ, UK

ARTICLE INFO

Handling Editor: Petar Sabev Varbanov

*Keywords:*
Synthetic kerosene
$CO_2$ to jet fuel
Fischer-tropsch
Methanol oligomerization
Aspen plus

ABSTRACT

Climate change and energy supply are major driving forces for the promotion of sustainable fuels production. In the aviation sector, due to inherent difficulties to adopt electrification methods for long distance flights, the successful implementation of sustainable aviation fuel (SAF) is crucial for the achievement of greenhouse gas emissions mitigation strategies. This study presents four different pathways for the valorization of captured $CO_2$ into synthetic kerosene using hydrogen and demonstrates the comparative assessment in terms of various technical and aspects such as hydrogen consumption, thermal energetic efficiency and produced e-kerosene quality. Two pathways are based on Fischer-Tropsch synthesis, a low-temperature CO conversion though reverse water-gas shift reaction and a high-temperature direct $CO_2$ conversion, while the other two are based on the valorization and upgrading of light alcohols (methanol and ethanol) derived from $CO_2$ hydrogenation. The process models were developed in Aspen Plus. Simulation results revealed that the low-temperature CO conversion pathway is the most efficient to maximize jet fuel yield with the lower energy and exergy losses. Indicatively for that case, 90.7% of the initial carbon is utilized for kerosene fraction synthesis, the overall thermal efficiency is 70.9% whereas the plant exergetic efficiency is 72.6%. The basic properties of the produced e-kerosene for all pathways meet with the required Jet-A1 specifications or are close to them.

## 1. Introduction

Low-carbon energy transition is a critical for a successful climate change mitigation [1]. Global warming and the climate change as a consequence of it have been recognized as of the most significant concerns that put the humanity and ecosystems survival on earth into danger. To avoid that, zero-emission technologies have to be fostered and rapidly deployed at commercial level in all sectors. Transportation is the third sector after energy and industry with the largest greenhouse gas (GHG) emissions [2] and the only one that increased its emissions the last 30 years in EU [3]. Unlike the road and railway transports that can eliminate their emissions through electrification, the aviation sector must rely only on the development of sustainable aviation fuels (SAF) as this is the only way for long distance flights to be carbon neutral since there is no alternative technology at high attitudes than the aircraft turbo engine.

The main types of SAFs, approved by ASTM (ASTM D7566 -20) as blending components for conventional jet fuel, are the Fischer-Tropsch synthetic paraffinic kerosene (FT-SPK), Fischer-Tropsch synthetic kerosene with aromatics (FT-SKA), Hydroprocessed Esters and Fatty Acids (HEFA), synthesized iso-paraffins (SIP), Alcohol to Jet (ATJ), catalytic hydrothermolysis (CHJ) and synthesized paraffinic kerosene from hydrocarbon-hydroprocessed esters and fatty acids (HC-HEFA-SPK), using feedstock from biological (advanced biofuels) or no-biological (e-kerosene) origin (see Fig. 1). Most of these routes produce paraffinic kerosene comprising blends of acyclic normal and branched alkanes [4]. Especially, for e-kerosene, renewable or low carbon electricity is needed for the production of hydrogen which is one of the main energy sources for the jet fuel like synthesis, this type of sustainable fuels are called electrofuels or e-fuels. Currently, the vast majority of SAF is produced through the HEFA from fats, oils and greases being Neste and World Energy the world leading companies for HEFA production at commercial-scale. Moreover, Gevo and LanzaJet have developed ATJ pathways for the production of renewable jet fuel from isobutanol and ethanol, respectively. The main bottleneck for these bio-based technologies is the high feedstock cost and low feedstock availability for large scale applications [5]. For that reason, the alternative way for SAF production using $CO_2$ and renewable $H_2$ as feedstock

* Corresponding author.
*E-mail address:* vasileios.inglezakis@strath.ac.uk (V.J. Inglezakis).

https://doi.org/10.1016/j.energy.2023.127868
Received 18 November 2022; Received in revised form 7 April 2023; Accepted 16 May 2023
Available online 23 May 2023

attracts the interest the last years.

There are several strategies to convert $CO_2$ and $H_2$ into liquid fuels mainly composed of hydrocarbons adopting either, biochemical, catalytic, electrochemical techniques or a combination of them. Due to the thermodynamic stability and chemical inertia of $CO_2$, its hydrogenation usually promotes the synthesis of short-chain compounds such as CO, methane, methanol, acetic acid and $C_2$–$C_4$ olefins, most of experimental studies are focused on the optimization of the synthesis process of these compounds. Hence, these options for synthetic kerosene synthesis are based on multi-stage pathways where $CO_2$ is firstly converted into an intermediate compound which in turn becomes the feedstock for the liquid hydrocarbons synthesis, in one or more process steps (Fig. 2). Nevertheless, there are studies that aim to produce liquid fuel directly from $CO_2$ with considerable selectivity to jet fuel fraction [6]. Currently, the most common pathway is to reduce $CO_2$ to CO either catalytically via the reverse water gas shift reaction (rWGS) [7], or electrochemically via a co-electrolysis pathway transforming water and $CO_2$ into syngas $H_2$/CO [8]. The first pathway consists of established technologies and has already been deployed at industrial scale [9]. Moreover, methanol attracts also the interest of the used feedstock for jet fuel production: recently ExxonMobil announces a novel technology based on that route [10].

Several studies that are dedicated to renewable liquid fuels synthesis using syngas and/or $CO_2$, as feedstock can be found in the literature. Most of these studies are not specifically addressing the synthesis of kerosene but the designs presented are suited for the production of several fuels such as diesel and gasoline. Sudiro and Bertucco [11] and Navas-Anguita et al. [12] present a process based on FT for the production of gasoline and diesel. Ruokonen et al. [13] present a process based on methanol-to-olefins and Mobil's Olefins to Gasoline and Distillate for the production of diesel (45%), kerosene (27%) and gasoline (17%). Konig et al. [14] design is based on FT and produces kerosene (43.9%), gasoline (31.2%) and diesel (24.9%). Petersen et al. [15] present a process based on ethanol and produce kerosene (59%), gasoline (37%) and diesel (4%). However, when the target is to produce sustainable aviation fuel, the gasoline and diesel are by-products with low impact value since the roadmap for zero-emissions in road transport is mainly based on vehicles electrification [10]. Another issue that is observed in most of the simulation studies for renewable jet fuel production is the restricted information that is given about the final products specifications. The general approach that is adopted is to represent

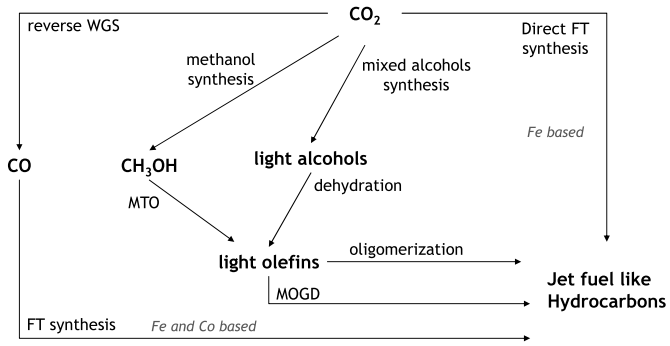


**Fig. 2.** Options for synthetic jet fuel synthesis from $CO_2$.

the final products with a model compound or a mix of them such as $C_{12}$–$C_{14}$ paraffins [16]. Taking, however, into account the strict standards for jet fuel specifications the appropriateness of each technology for the production of SAF is strongly affected by the target to meet standards or the additional actions to be taken. The aim of this research is to study and simulate catalytically-based pathways specifically designed to maximize jet fuel production from $CO_2$, the main properties of which fall under the ASTM specifications for aviation fuels; a conventional low temperature Fischer-Tropsch, a novel, high temperature Fischer-Tropsch without a reverse water gas shift reactor, a novel methanol-based and a novel ethanol-based pathway. The four pathways are compared in terms of energy efficiency and process effectiveness while the produced jet fuels can be regarded as potential "drop-in" according to the ASTM specifications.

## 2. Approach and methodology

In this paper, four thermocatalytic pathways are developed and the respective flowsheets are designed in such way that the jet fuel yield is maximized and the rest fuel fractions are eliminated. Three pathways are based on $CO_2$ conversion into intermediate compound such CO and methanol whereas one is based on the conversion of $CO_2$ to medium chain hydrocarbons in one step. Since the focus of this study is to identify the most effective transformation of $CO_2$ into jet fuel, the way that hydrogen and pure $CO_2$ stream are produced or supplied in the plant are not taken into account. The origin of $CO_2$ plays decisive role in

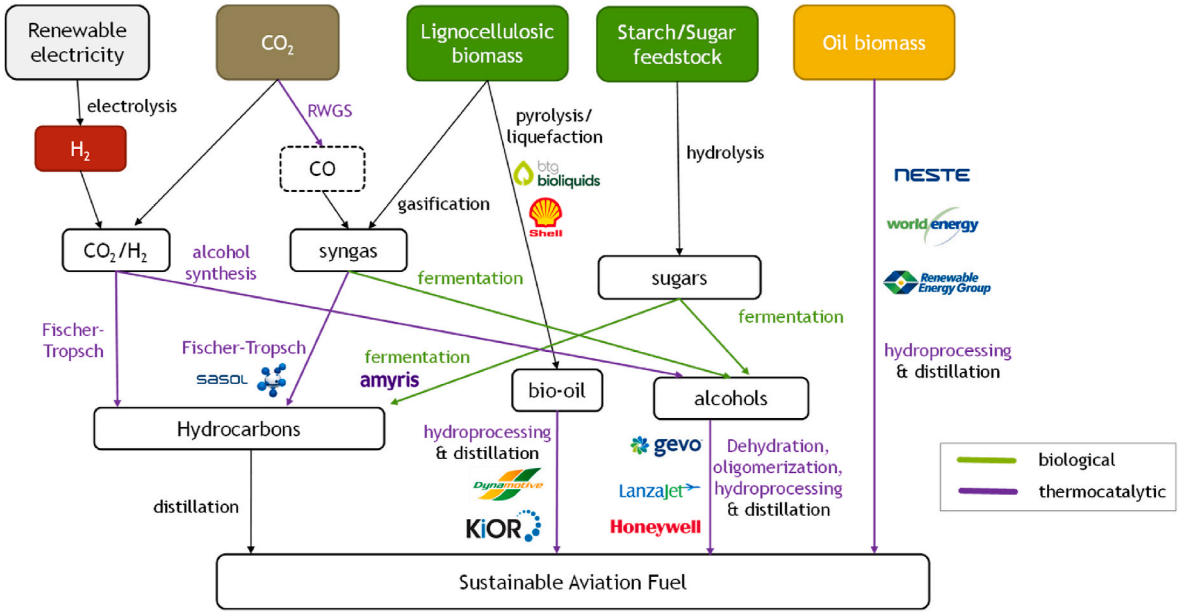


**Fig. 1.** Available pathways for SAF production.

the GHG footprint of the final products. The $CO_2$ either can come from the atmosphere (Direct Air Capture) or can have biogenic (from bio-energy or biorefinery plant) or fossil carbon origin (industrial flue gases). In any case, the $CO_2$ stream that will be used for the synthetic kerosene production must meet certain specifications in terms of gas impurities (i.e. nitrogen oxides, oxygen gas, sulfur oxides and hydrocarbons) concentration to avoid the reactors catalysts poisoning. In all the examined cases, the $CO_2$ flow rate is set equal to 100 kmol/h whereas the hydrogen consumption is left as a dependent variable. This $CO_2$ flow rate corresponds to an annual $CO_2$ valorization of 40 kt/y and an electrolyser capacity of 30–50$MW_e$. This size selection has been done arbitrarily and although it corresponds to a rather small industrial scale unit the overall process is definitely scalable and can be applied at larger scales. The proper size determination is a matter of the techno-economic assessment, which is not part of that study. As far as the process analysis in concerned, this is mainly based on the process simulation modeling of the examined flowsheets performed with Aspen Plus. The reactors modeling was based either on the assumption of the chemical equilibrium or on data from published experimental data.

### 2.1. Definition of performance indicators

The following metrics are introduced for the performance evaluation of each case.

The Carbon Utilization (CU) determines the portion of initial carbon that exist in the form of $CO_2$ that is finally found in the synthetic kerosene stream.

$$CU = \frac{\dot{n}_{C,e-jet}}{\dot{n}_{C,CO2in}} \quad \text{eq 1}$$

where $\dot{n}_{C,e-jet}$ the carbon molar flow (kmol/h) at the produced jet fuel stream and $\dot{n}_{C,CO2in}$ the C flow (kmol/h) at the $CO_2$ inlet stream.

The Energetic Jet Fuel Efficiency (EJFE) measures the thermal efficiency of the process and the ratio of heat input of the produced SAF (MW on a LHV base) to the total used hydrogen heat input plus the external heat ($Q_{ext}$) if necessary:

$$EJFE = \frac{\dot{m}_{e-jet} \bullet LHV_{e-jet}}{\dot{m}_{H2,in} \bullet LHV_{H2} + Q_{ext}} \quad \text{eq 2}$$

In order to take into account all the external heating and power demands for the effective and stable operation of the proposed systems the term of overall plant efficiency ($\eta_{tot}$) is defined as:

$$\eta_{tot} = \frac{\dot{m}_{e-jet} \bullet LHV_{e-jet}}{\dot{m}_{H2,in} \bullet LHV_{H2} + Q_{ext} + P_{ext}} \quad \text{eq 3}$$

For the cases where refrigeration loads are required, the respective loads are converted into electricity, assuming a constant coefficient of performance (COP) of 3.14 [17].

The e-kerosene yield ($Y_{e\text{-}jet}$) defines the amount of produced synthetic aviation fuel mass flow ($\dot{m}_{e-jet}$) to the inlet $CO_2/H_2$ feed gas mass flow ($\dot{m}_{H2,in} + \dot{m}_{CO2,in}$):

$$Y_{e-jet} = \frac{\dot{m}_{e-jet}}{\dot{m}_{H2,in} + \dot{m}_{CO2,in}} \quad \text{eq 4}$$

The e-kerosene fraction ($f_{\text{e-jet}}$) defines the portion of the produced synthetic aviation fuel mass flow among the mass flow of other side products (i.e. diesel and gasoline):

$$f_{e-jet} = \frac{\dot{m}_{e-jet}}{\dot{m}_{products,tot}} \quad \text{eq 5}$$

### 2.2. Exergy analysis

The methodological tool of exergy analysis is employed in order to have a more qualitative assessment of the examined schemes by considering the available energy of the main inlet and outlet streams. A term of exergy efficiency is introduced that is defined as the ratio of total exergy output of the useful streams (i.e. liquid products) to total exergy input:

$$\eta_{Ex} = \frac{\dot{E}_{jet\ fuel} + \dot{E}_{Diesel+gasoline}}{\dot{E}_{H2,in} + \dot{E}_{CO2,in} + \dot{P}_{in} + \dot{E}_{Q,in}} \quad \text{eq 6}$$

where $\dot{E}_{jet\ fuel}$ and $\dot{E}_{Diesel+gasoline}$ (in MW) are the chemical exergies of the final liquid fuels calculated according to the following equation [18]:

$$\dot{Ex}_{liquid\ fuel} = N \bullet \varepsilon_{ch} = N \bullet \left( \sum x_i \varepsilon_{o,i} + RT \sum x_i ln x_i \right) \quad \text{eq 7}$$

where $N$ is the molar flow in kmol/s and $x_i$ the molar fraction of each component $i$. The reference conditions used are the standard environmental conditions ($T_o = 298.15$ K, $p_o = 1.013$ bar) and values of $\varepsilon_{0,i}$ for each component are obtained from Ref. [19].

Exergy of power equals power itself and exergy of a heat stream $Q$ ($\dot{E}_{Q,i}$) is evaluated with the help of the Carnot factor:

$$\dot{E}_{Q,i} = Q_i \bullet \left(1 - \frac{T_0}{T_i}\right) \quad \text{eq 8}$$

where $T_i$ is the temperature at which $Q_i$ is available and $i$ = in or out.

The overall exergy that is destructed according to the second thermodynamic law ($\dot{E}_{loss}$) is calculated from the exergy balance of the overall system (see Fig. 3):

$$\dot{E}_{loss} = \left(\dot{E}_{H2,in} + \dot{E}_{CO2,in} + \dot{P}_{in} + \dot{E}_{Q,in}\right) - \left(\dot{E}_{jet\ fuel} + \dot{E}_{Diesel+gasoline} + \dot{E}_{Q,waste\ heat}\right) \quad \text{eq 9}$$

The term $\eta_{wasted}$ expresses the amount of exergy that is wasted in the form of unexploited heat to the total exergy input:

$$\eta_{wasted} = \frac{\dot{E}_{Q,waste\ heat}}{\dot{E}_{H2,in} + \dot{E}_{CO2,in} + \dot{P}_{in} + \dot{E}_{Q,in}} \quad \text{eq 10}$$

Whereas the term $\eta_{loss}$ expresses the ratio of irreversibilities ($E_{loss}$) of the overall process to the total exergy input:

$$\eta_{loss} = \frac{\dot{E}_{loss}}{\dot{E}_{H2,in} + \dot{E}_{CO2,in} + \dot{P}_{in} + \dot{E}_{Q,in}} \quad \text{eq 11}$$

## 3. Pathways description

### 3.1. FT based pathways

In this work, as is the common practice in plant level simulation studies, only the main FT reactions were considered. This approach is followed in conceptual design and simulation studies to avoid unnecessary complexity which can lead to convergence problems, as the production of other organic groups such as alcohols, aldehydes and acids have negligible impact on the overall process.

#### 3.1.1. High-temperature Fischer-Tropsch synthesis without rWGS (CO2FT)

The available studies on high-temperature Fischer-Tropsch (FT) synthesis without separate reverse water-gas shift (rWGS) reactor are rare and are limited to laboratory experimental research. This process is called non-methanol mediated $CO_2$ hydrogenation [20] and combines

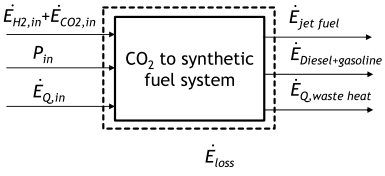


**Fig. 3.** Exergy balance.

FT and rWGS reactions in a single reacrtor by use of Fe catalysts. The reactions considered are [21]:

$$CO_2 + H_2 \Longleftrightarrow CO + H_2O \quad (12)$$

$$nCO + (2n+1)H_2 \Longleftrightarrow C_nH_{2n+2} + nH_2O \quad (13)$$

$$nCO + 2nH_2 \Longleftrightarrow C_nH_{2n} + nH_2O \quad (14)$$

To reach satisfactory $CO_2$ conversions and $C_5$–$C_{15}$ yields it is necessary to use high temperature, pressure and excess $H_2$ in combination to a catalyst that suppresses $CH_4$ production [22]. In the present paper experimental data of a Fe-based catalyst containing K as a promoter were used [23].

The process flow diagram is shown in Fig. 4. The FT reactor product is cooled and sent to adsorption units for the removal of $CO_2$ and $H_2$ and then is decanted to separate water, light gases and the hydrocarbons. The light gases are recompressed and sent to an oligomerization reactor where the light olefins ($C_2$–$C_9$) are dimerized. The products are sent to a flash drum where the gases and olefins are separated. The gases are sent to a $H_2$ adsorption unit, a flash drum to separate the remaining olefins and then to an autothermal reactor (ATR). Reforming of light gases, mainly $CH_4$, produces syngas and increases overall conversion [24]. The main reactions are [25]:

$$CH_4 + 3/2\ O_2 \Longleftrightarrow CO + H_2O \quad (15)$$

$$CH_4 + H_2O \Longleftrightarrow CO + 3H2 \quad (16)$$

$$CO + H_2O \Longleftrightarrow CO_2 + H2 \quad (17)$$

Besides $CH_4$ all light hydrocarbons are converted to syngas. The excess $H_2O$ is separated in a flash drum and the syngas is mixed with fresh $CO_2$ and $H_2$. The hydrocarbons separated at the decanter and the olefins produced in the oligomerization reactor are sent to a hydrotreater where olefins are transformed to paraffins and heavy paraffins ($C_{24+}$) are cracked to smaller paraffins. The products are sent to adsorption units for the removal of $CO_2$ and $H_2$ and then to the first distillation column where kerosene is taken at the bottom and the lighter hydrocarbons at the top. The top product is sent to a second distillation column where gasoline is taken at the bottom and light tail gas at the top. The latter is sent to the ATR for reforming.

As seen in Table 1, all the reaction processes take place under high pressure and temperature. All reactors apart from ATR produce excess heat because of the exothermic nature of the reactions that are carried out. The excess heat is utilized either for the effective preheating other streams or for low pressure (LP) steam generation. The same strategy is also followed in the remaining cases.

### 3.1.2. Low-temperature Fischer-Tropsch synthesis (LTFT)

In the examined pathway, $CO_2$ is firstly transformed into CO in the rWGS reactor:

$$CO_2 + H_2 \Longleftrightarrow CO + H_2O \quad (18)$$

The transformation of $CO_2$ to CO is thermodynamically favored by high temperature because it is reversible and endothermic and is pressure independent. The rWGS is always accompanied by undesired $CO_2$ methanation, also called the Sabatier reaction, which is exothermic, favored by lower temperature and high pressure [26]:

$$CO_2 + 4H_2 \Longleftrightarrow CH_4 + 2H_2O \quad (19)$$

Hence to maximize the CO production low pressures and high temperatures are required. The process flow diagram is shown in Fig. 5. The rWGS reactor products are sent to flash where water is separated and then to an adsorber for the removal of $CO_2$. The syngas compressed and then is transformed into hydrocarbons by low-temperature Fischer-Tropsch (FT) synthesis (LTFT). When Co is used as catalyst in LTFT, it is commonly assumed that only paraffins are produced and the main reaction is accompanied by the water-gas shift reaction (WGS) [27–29]:

$$nCO + (2n+1)H_2 \Longleftrightarrow C_nH_{2n+2} + nH_2O \quad (20)$$

$$CO + H_2O \Longleftrightarrow CO_2 + H2 \quad (21)$$

The FT reactor product is cooled and decanted to separate water, light gases and the hydrocarbons. The light gases are recompressed and sent to a $H_2$ adsorption unit and then to an autothermal reforming reactor (ATR). The excess $H_2O$ is separated in a flash drum and the syngas is mixed with fresh $CO_2$ and $H_2$. The hydrocarbons are sent to a hydrocracker where the heavier molecules are broken to lighter molecules [28]:

$$C_{2n}H_{4n+2} + H_2 \Longleftrightarrow 2C_nH_{2n+2}\ (C_{24}\text{ and }C_28) \quad (22)$$

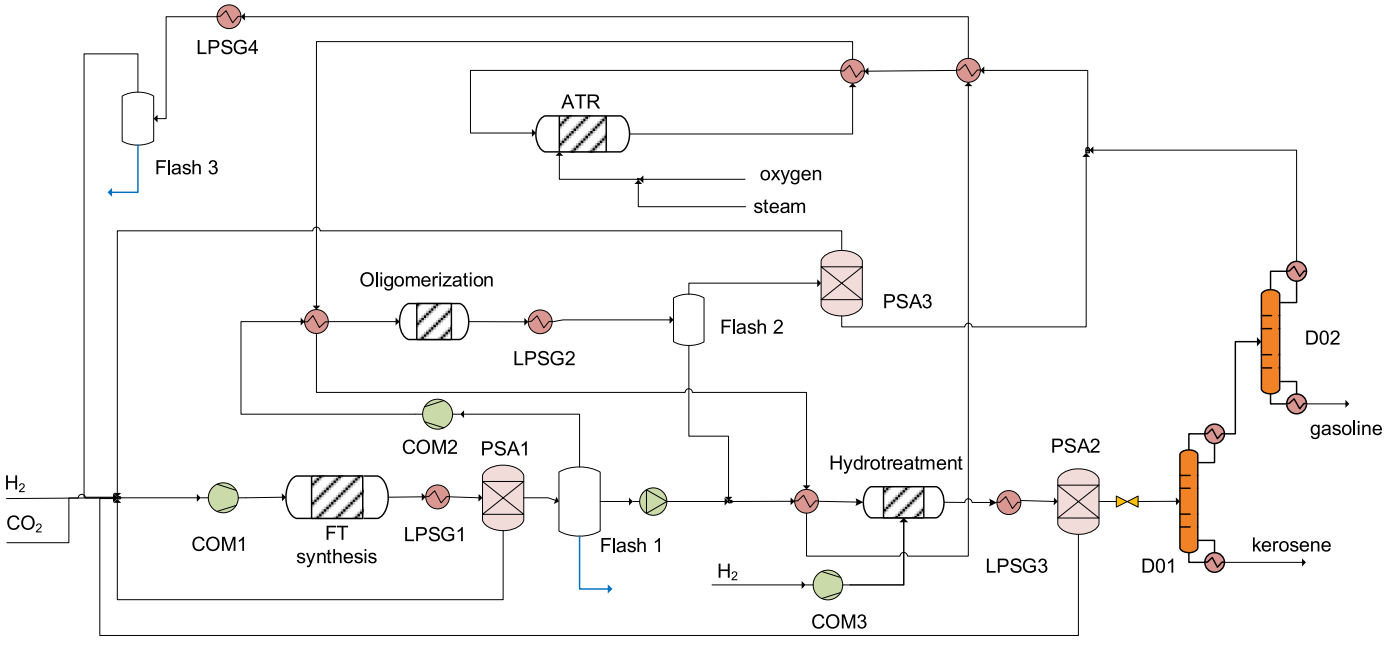


**Fig. 4.** Process flowsheet of the $CO_2$ to Jet fuel pathway via CO2FT (direct $CO_2$ into FT liquids).

**Table 1**
Flash separators and distillation columns process specifications.

| CO2FT | | | |
|---|---|---|---|
| Flash 1 | T = 30 °C, p = 25 bar | Distil 1 | $N_{tot}$ = 10, $N_{feed}$ = 5, BR = 1.16, RR = 0.5 |
| Flash 2 | T = 40 °C, Δp = 0 bar | Distil 2 | $N_{tot}$ = 10, $N_{feed}$ = 5, BR = 4.08, RR = 3 |
| Flash 3 | T = 40 °C, p = 5 bar | | |
| **LTFT** | | | |
| Flash 1 | T = 30 °C, p = 5 bar | Distil 1 | $N_{tot}$ = 10, $N_{feed}$ = 5, BR = 3, RR = 0.735 |
| Flash 2 | T = 30 °C, Δp = 0 bar | Distil 2 | $N_{tot}$ = 20, $N_{feed}$ = 10, BR = 40.99, RR = 2 |
| Flash 3 | T = 30 °C, p = 5 bar | | |
| **MeOH based** | | | |
| Flash 1 | Q = 0, Δp = 0.15 bar | Distil 1 | $N_{tot}$ = 35, $N_{feed}$ = 30, BR = 0.54, RR = 1.22 |
| Flash 2 | Q = 0, Δp = 0 bar | Distil 2 | $N_{tot}$ = 40, $N_{feed}$ = 12, BR = 2.94, RR = 0.89 |
| Flash 3 | T = 28 °C, Δp = 0 bar | Distil 3 | $N_{tot}$ = 30, $N_{feed}$ = 10, BR = 4.11, RR = 0.36 |
| Flash 4 | Q = 0, Δp = 0 bar | Distil 4 | $N_{tot}$ = 10, $N_{feed}$ = 3, BR = 28.3, RR = 1.5 |
| Flash 5 | T = 30 °C, Δp = 4 bar | Distil 5 | $N_{tot}$ = 10, $N_{feed}$ = 11, BR = 0.56, RR = 1.14 |
| Flash 6 | Q = 0, Δp = 0 bar | | |
| Flash 7 | T = 28 °C, Δp = 0 bar | | |
| **EtOH based** | | | |
| Flash 1 | T = −18 °C, Δp = 0 bar | Distil 1 | $N_{tot}$ = 20, $N_{feed}$ = 8, BR = 0.60, RR = 0.31 |
| Flash 2 | Q = 0, Δp = 0 bar | Distil 2 | $N_{tot}$ = 35, $N_{feed}$ = 14, BR = 1.37, RR = 3.14 |
| | | Distil 3 | $N_{tot}$ = 3, $N_{feed}$ = 1, BR = 0.45, RR = 0 |
| | | Distil 4 | $N_{tot}$ = 30, $N_{feed}$ = 14, BR = 6.62, RR = 6.33 |
| | | Distil 5 | $N_{tot}$ = 70, $N_{feed}$ = 41, BR = 4.55, RR = 1.48 |
| | | Distil 6 | $N_{tot}$ = 5, $N_{feed}$ = 3, BR = 5.79, RR = 0.67 |

$N_{tot}$: number of stages, $N_{feed}$: stage number of feed stream, BR: boilup ratio, RR: reflux ratio.

$$C_{4n}H_{8n+2} + 3H_2 \Longleftrightarrow 4C_nH_{2n+2}\ (C_{32} - C_{64}) \quad (23)$$

Following hydrocracking the hydrocarbons are sent to a $H_2$ adsorption unit and then to the first distillation column where light hydrocarbons are taken at the top and sent to the ATR and heavy hydrocarbons at the bottom. The heavy hydrocarbons are sent to a second distillation column where kerosene is taken at the top and diesel at the bottom.

It should be underlined that in both FT-based pathways, it is assumed that hydrocarbons ($C_xH_y$) is the only organic compounds group that are found in the FT reactor outlet. Since some experimental studies report the formation of alcohols and acids, there are certain methodologies like the use of adsorbents [30]or tripper-sidestream decanter [31] that can effectively remove them from the FT crude stream.

### 3.2. Light alcohols-based pathways

#### 3.2.1. Methanol-based pathway

In this pathway, $CO_2$ is firstly transformed into methanol which is subsequently converted into medium/long chain hydrocarbons through a series of catalytic processes. The methanol synthesis through $CO_2$ hydrogenation is carried out according to the reactions:

$$CO + 2H_2 \Longleftrightarrow CH_3OH \quad (24)$$

$$CO_2 + H_2 \Longleftrightarrow CO + H_2O \quad (25)$$

$$CO_2 + 3H_2 \Longleftrightarrow CH_3OH + H_2O \quad (26)$$

The process flow diagram of a typical methanol synthesis unit from $CO_2$ is shown in Fig. 6. The unit consists of the methanol synthesis, gas separation and product purification. The inlet gas is heated up to a certain temperature level. The required heat for crude methanol heating and separation is obtained from the gas outlet cooling and the excess heat from the methanol synthesis reactor (exothermic process). In order to achieve high purity levels in the methanol product (>99.2%), the liquid stream after the first flash separator is throttled down to atmospheric pressure. A small portion (0.5%) of the recycling gas is extracted as purge gas in order to avoid by-products accumulation such as hydrocarbons, inert gas etc.

The rationale behind that is based on the separate handling of each light olefin as it is produced at the methanol-to-olefins (MTO) reactor aiming to maximize the yield of the desired hydrocarbons within the range of C12–C14. The main units of that pathway is a) the MTO unit, b) the olefins oligomerization unit c) the oligomers hydrotreatment and d) the ATR unit. The produced methanol enters the MTO reactor and the produced light olefins/paraffins are recovered according to the UOP/Hydro MTO pathway [32]. The light gases are recovered and sent to ATR for reforming. The olefins (i.e. ethylene, propylene and butylene) are sent for oligomerization.

The recovered ethylene undergoes dimerization for the production of 1-butene. The reaction parameters for this process were obtained from Ref. [33]. The recovered 1-butene mixes with the product stream from ethylene dimerization and undergo oligomerization (mainly dimerization and trimerization). The process parameters and the associated

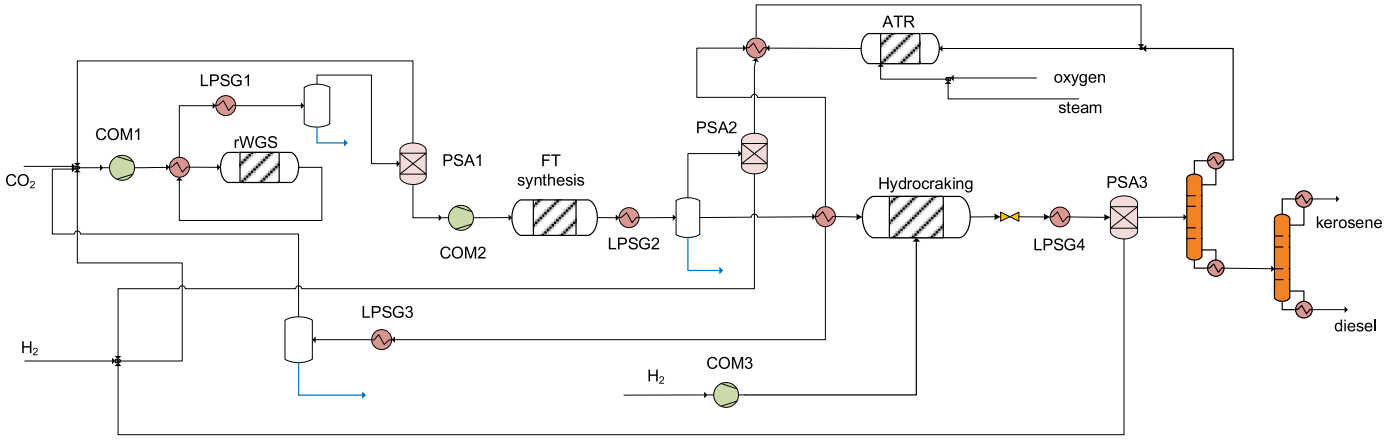


**Fig. 5.** Process flowsheet of the $CO_2$ to Jet fuel pathway via LTFT (through rWGS).

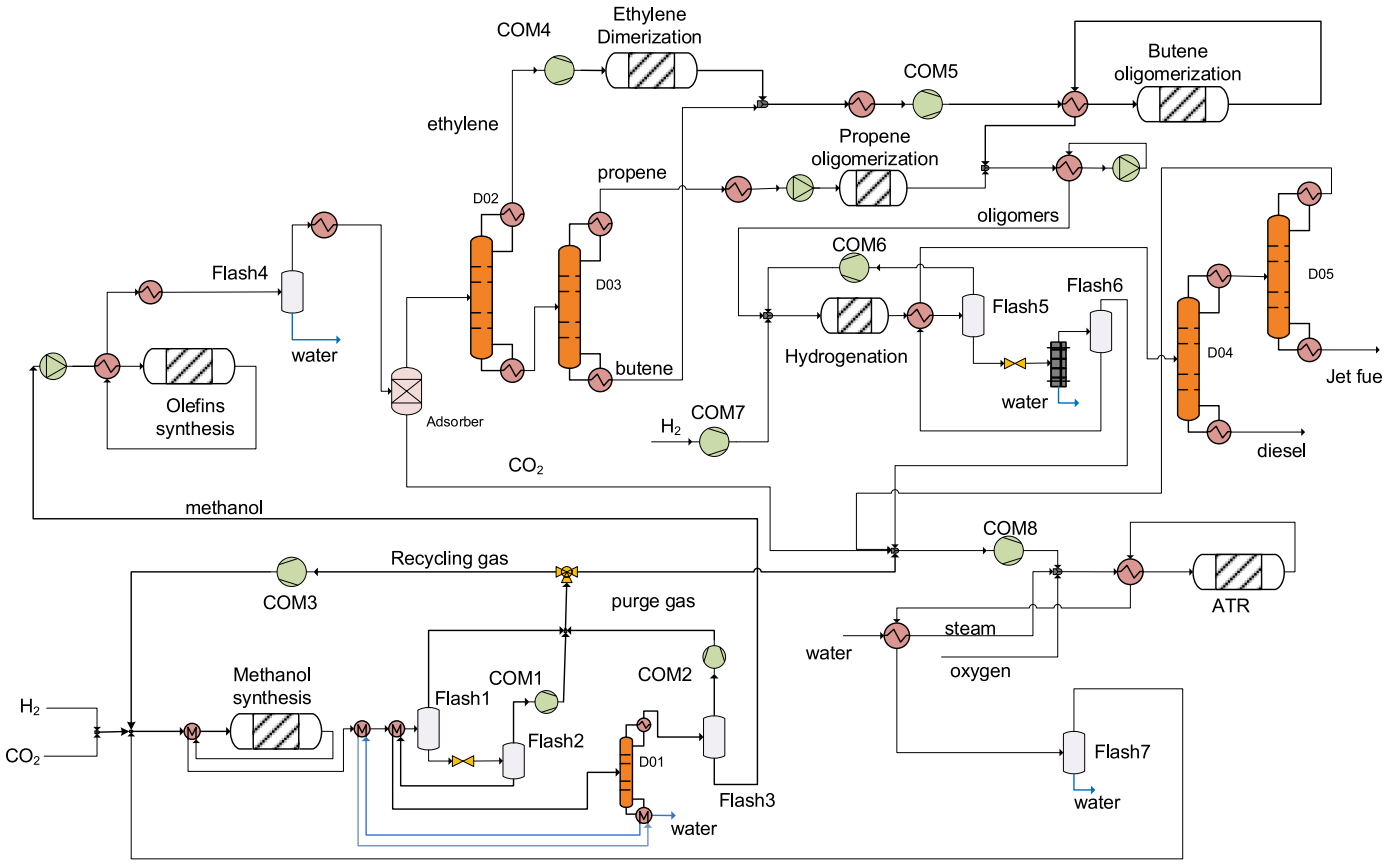


**Fig. 6.** Process flowsheet of the $CO_2$ to Jet fuel pathway via methanol synthesis.

reactions were obtained from Ref. [34]. The recovered propene undergoes oligomerization for the production of various oligomers (dimers, trimers, tetramers, etc.). The process parameters and the associated reactions were obtained from Ref. [35]. All the produced oligomers mix and send to the hydrotreatment unit for hydrogenation and their conversion into alkanes. The same reactor that has been employed in the MTO/MOGD pathway was used, enriched with the respective hydrogenation reactions of the olefins that are not considered in the former scenario (i.e. same conversion rate = 90%). The Autothermal Reformer (ATR) reactor is pressurized, oxygen blown, in order to avoid some of the compression duty of the recycling gas and to exploit the oxygen that is produced as the electrolyser together with the hydrogen.

### 3.2.2. *Ethanol-based pathway*

Fig. 7 present the process flow diagram of the fourth pathway.

The main idea of this pathway is to transform $CO_2$ into ethanol and the latter to be the basis for the medium/long chain hydrocarbons based on an alcohol-to-jet (ATJ) scheme. The fresh $H_2/CO_2$ stream after compression is mixed with the recycling streams (internal gas loop, external gas loop coming from the Ethanol Synthesis unit and methanol) and undergoes dimethyl ether (DME) synthesis:

$$CO_2 + H_2 \Longleftrightarrow CO + H_2O \tag{27}$$

$$CO_2 + 3H_2 \Longleftrightarrow CH_3OH + H_2O \tag{28}$$

$$2CH_3OH \Longleftrightarrow CH_3O\,CH_3 + H_2O \tag{29}$$

In order to produce DME in one step, bifunctional catalysts should be applied, where the first reaction is catalyzed by an acidic catalyst such HZSM-5 and the rest two by a methanol synthesis catalyst such as $Cu/ZnO/Al_2O_3$ [36].

The produced DME is recovered after a subsequent distillation column and a flash separator whereas the unconverted methanol is separated from water in a second column. Part of the unreacted gas is split and mixed with DME that is needed for the Ethanol synthesis according to the following set of reactions.

$$CH_3O\,CH_3 + CO \Longleftrightarrow CH_3COOCH3 \tag{30}$$

$$CH_3COOCH_3 + 2H_2 \Longleftrightarrow CH_3OH + CH_3CH_2OH \tag{31}$$

The first is the DME carbonylation where methyl acetate (MA) is formed in the presence of H-Mordenite (H-MOR) zeolite, whereas the second one is the produced ester hydrogenation over the Cu/ZnO catalyst. The reactions take place in a dual bed reactor sequentially, at 15 bar and 220 °C. Moreover, $CO_2$ and ethyl acetate (EA) are also by-products [37]. After the products separation, DME, MA and EA reenter to the reactor, whereas the $CH_3OH$ and $CO_2$ are sent at the DME synthesis unit. To accomplish that, a series of two distillation columns and a flash separation is employed as seen in Fig. 7. This way of producing synthetic ethanol from $CO_2$ has been introduced earlier in Ref. [38] and is adopted it again in the present study as the direct catalytic conversion of $CO_2$ into ethanol does not yield high conversion and selectivity rates together, according to the recent relevant studies [39].

The third section of the process consists of the ethanol upgrade into medium/long chain hydrocarbons based on four consecutive catalytic reactions: ethanol condensation, n-butanol dehydration, light olefins oligomerization, and oligomers hydrogenation [40]. In the first step, ethanol is converted into n-butanol according to the following Guerbet reaction:

$$2C_2H_5OH \rightarrow C_4H_9OH + H_2O \tag{32}$$

High ethanol conversion rates and selectivity in n-butanol can be achieved if a catalyst such as $RuCl_2$ is applied [41]. Apart from butanol,

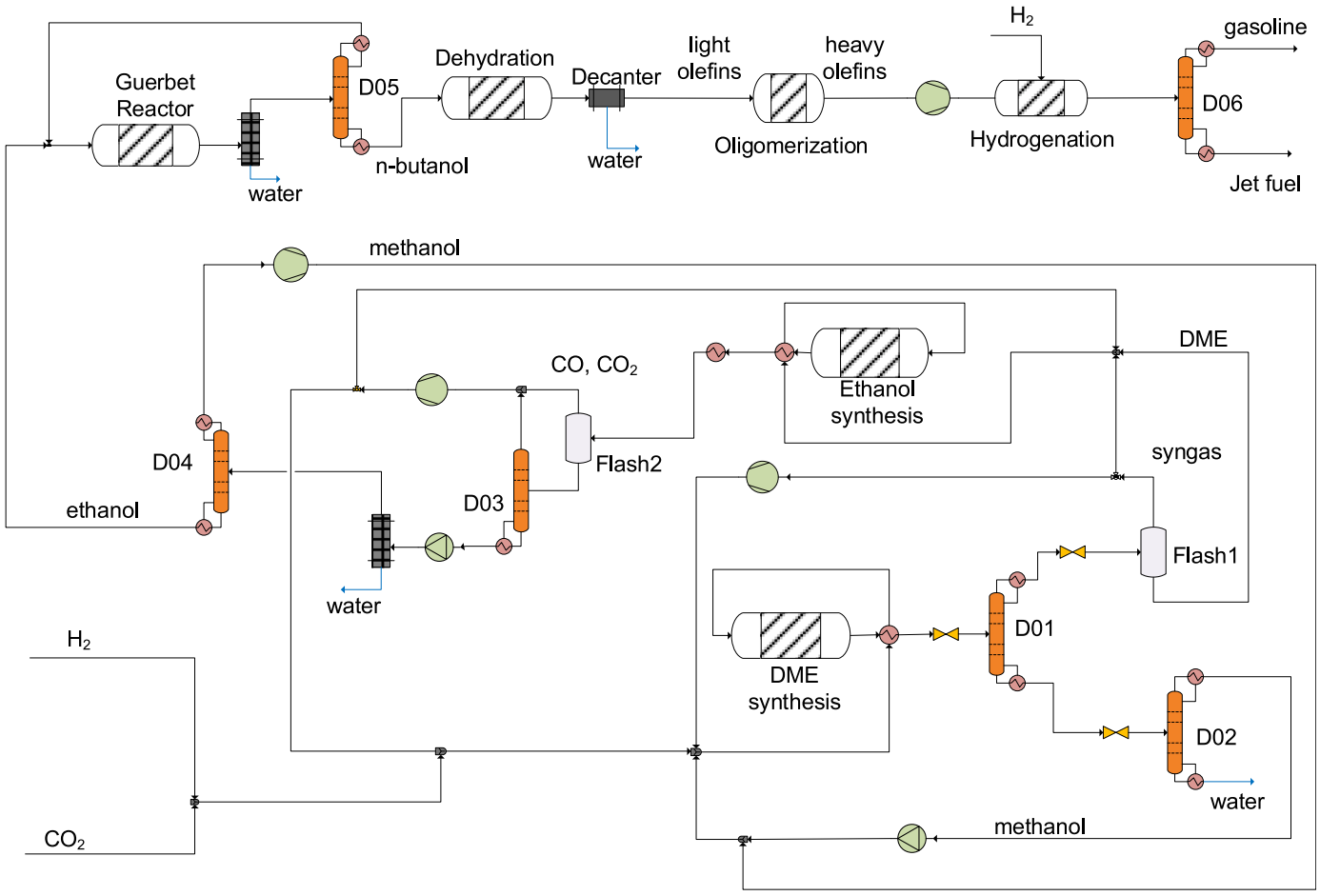


**Fig. 7.** Process flowsheet of the $CO_2$ to Jet fuel pathway via DME/ethanol synthesis.

hexanol and 2-ethyl hexanol are also produced as by-products. In the second reaction step, the produced alcohols undergo dehydration and the respective alkenes are produced which in turn are converted into oligomers in the third reactor. The last catalytic process is the hydrotreatment of all the produced alkenes for the production of paraffinic hydrocarbons that will be the basic compounds of the final fuel products. As depicted in Fig. 7, each catalytic step is followed by the necessary separation step for the removal of impurities or the recovery of the desired products.

## 4. Process model methodology

The flowsheets development and the process simulations were performed in Aspen Plus. The following subsections present the methodology for the main reactors modeling in each case. Regarding the rest components, a strategy of using the same specifications: the compressors isentropic efficiency is set at 85%, the pumps efficiency at 70% and the $H_2$ recovery efficiency at PSA unit is 99%, retrieving 100% pure hydrogen. The process specifications of the flash separators and distillation columns are summarized in Table 1.

Moreover, the heat demands or the excess heat removal are fulfilled by external utilities, the specification of which are uniform for all the examined cases. Table 2 presents their basic characteristics. The refrigerants are considered as a separate utility but the required power for their generation is also taken into account in the energy analysis.

### 4.1. High-temperature Fischer-Tropsch synthesis (CO2FT)

Table 3 presents the models parameters that are used for the reactors simulation. In the present paper experimental data of a Fe-based (10Fe0·8 K) catalyst were used with an overall $CO_2$ conversion of 0.417 [23]. For this catalyst and the specific operational conditions (300 °C, 25 bar, $H_2/CO_2 = 3$) the fractional selectivity of light hydrocarbons and CO were estimated based on the experimental data: $CH_4 = 0.103$, $C_2H_4 = 0.072$, $C_2H_6 = 0.0207$, $C_3H_6 = 0.072$, $C_3H_8 = 0.0207$, $C_4H_8 = 0.072$, $C_4H_{10} = 0.0207$ and $CO = 0.06$. The distribution of the $C_{4+}$ paraffins in the FT reactor is calculated through the Anderson-Schulz-Flory (ASF) distribution which define the stoichiometry of the overall reaction or the selectivity of the products. The chain growth probability factor (α) for $CO_2$FT is between 0.57 and 0.79 depending on the carbon number and the value of 0.72 was used in this paper [42]. The distribution of $C_{4+}$ olefins was based on this of the respective paraffins and the following olefin/paraffin ratio [43]: 18.9/6.8 for $C_5$–$C_{11}$, 14.8/3.8 for $C_{12}$–$C_{20}$ and 1.8/0.5 for $C_{24}$ and $C_{28}$. Stoichiometric amount of $H_2$ was fed to the hydrotreater. Combustion in an ATR is sub-stoichiometric with an overall oxygen to hydrocarbon ratio of 0.55–0.6 [25]. Reforming and WGS reactions take place in the

**Table 2**
Utilities specifications.

| Type of utility | Temperature (°C) | Use |
|---|---|---|
| Very High T source | 1000 | Hot |
| Fired Heat | 400 | Hot |
| HP/IP/LP Steam | 250/175/125 | Both Hot & Cold |
| Air ventilation | 30 | Both Hot & Cold |
| Cooling Water | 20 | Cold |
| Refrigerant 1/2/3 | −25/-40/-65 | Cold |

**Table 3**
Reactors models specifications for the CO2FT pathway.

| Reactor name | Reactor model | Process specifications | Associated reactions | Fractional conversion |
|---|---|---|---|---|
| Fischer-Tropsch | RSTOIC | 300 °C/25 bar $H_2/CO_2 = 3$ | $CO_2 + H_2 \Longleftrightarrow CO + H_2O$ nCO + (2n+1)$H_2 \Longleftrightarrow C_nH_{2n+2} + nH_2O$ nCO + 2n$H_2 \Longleftrightarrow C_nH_{2n} + nH_2O$ | 0.417 ($CO_2$) |
| Oligomerization | RSTOIC | 350 °C/40 bar | $2C_2H_4 \rightarrow C_4H_8$ | 1 |
| | | | $2C_3H_6 \rightarrow C_6H_{12}$ | 1 |
| | | | $2C_4H_8 \rightarrow C_8H_{16}$ | 1 |
| | | | $2C_5H_{10} \rightarrow C_{10}H_{20}$ | 1 |
| | | | $2C_6H_{12} \rightarrow C_{12}H_{24}$ | 0.85 |
| | | | $2C_7H_{14} \rightarrow C_{14}H_{28}$ | 0.85 |
| | | | $2C_8H_{16} \rightarrow C_{16}H_{32}$ | 0.8 |
| | | | $2C_9H_{18} \rightarrow C_{18}H_{36}$ | 0.8 |
| Hydrotreater | RSTOIC | 300 °C/30 bar | $C_3H_6 + H_2 \rightarrow C_3H_8$ | 0.9 |
| | | | $C_4H_8 + H_2 \rightarrow C_4H_{10}$ | 0.9 |
| | | | $C_5H_{10} + H_2 \rightarrow C_5H_{12}$ | 0.9 |
| | | | $C_6H_{12} + H_2 \rightarrow C_6H_{14}$ | 0.9 |
| | | | $C_7H_{14} + H_2 \rightarrow C_7H_{16}$ | 0.9 |
| | | | $C_8H_{16} + H_2 \rightarrow C_8H_{18}$ | 0.9 |
| | | | $C_9H_{18} + H_2 \rightarrow C_9H_{20}$ | 0.9 |
| | | | $C_{10}H_{20} + H_2 \rightarrow C_{10}H_{22}$ | 0.9 |
| | | | $C_{11}H_{22} + H_2 \rightarrow C_{11}H_{24}$ | 0.9 |
| | | | $C_{12}H_{24} + H_2 \rightarrow C_{12}H_{26}$ | 0.9 |
| | | | $C_{13}H_{26} + H_2 \rightarrow C_{13}H_{28}$ | 0.9 |
| | | | $C_{15}H_{30} + H_2 \rightarrow C_{15}H_{32}$ | 0.9 |
| | | | $C_{16}H_{32} + H_2 \rightarrow C_{16}H_{34}$ | 0.9 |
| | | | $C_{17}H_{34} + H_2 \rightarrow C_{17}H_{36}$ | 0.9 |
| | | | $C_{18}H_{36} + H2 \rightarrow C_{18}H_{38}$ | 0.9 |
| | | | $C_{19}H_{38} + H_2 \rightarrow C_{19}H_{40}$ | 0.9 |
| | | | $C_{20}H_{40} + H_2 \rightarrow C_{20}H_{42}$ | 0.9 |
| | | | $C_{24}H_{50} + H_2 \rightarrow 2C_{12}H_{26}$ | 1 |
| | | | $C_{24}H_{48} + 2H_2 \rightarrow 2C_{12}H_{26}$ | 1 |
| | | | $C_{28}H_{58} + H_2 \rightarrow 2C_{14}H_{30}$ | 1 |
| | | | $C_{28}H_{56} + 2H_2 \rightarrow 2C_{14}H_{30}$ | 1 |
| | | | $C_{48}H_{98} + 3H_2 \rightarrow 4C_{12}H_{26}$ | 1 |
| | | | $C_{48}H_{96} + 4H_2 \rightarrow 4C_{12}H_{26}$ | 1 |
| Autothermal reactor | RGIBBS | 950 °C/5 bar $O_2/C = 0.7$ $H_2O/C = 4$ | – | – |

The distillation columns are modeled as RADFRAC. The Peng-Robinson property method with Boston-Mathias modification is selected with STEAMNBS as free water method.

catalytic zone of the reactor by using steam with $H_2O/C$ ratios ranging from 0.2 to 3.5 [44]. In this study, the estimated optimum $O_2/C$ and $H_2O/C$ molar ratios were 0.7 and 4, respectively.

### 4.2. Low-temperature Fischer-Tropsch synthesis (LTFT)

Table 4 presents the models parameters that are used for the reactors simulation. The $H_2/CO$ molar ratio at the FT reactor inlet was kept equal to 2 in order to maximize the selectivity for hydrocarbons within the kerosene chain length [45]. The overall CO conversion was set to 0.85. The distribution of the $C_{4+}$ hydrocarbons in the FT reactor is calculated through the Anderson-Schulz-Flory (ASF) distribution which define the stoichiometry of the overall reaction or the selectivity of the products. The chain growth probability factor (α) depends on the process conditions and in this paper the value of 0.92 was used [27]. The ASF distribution fails to represent the data for light hydrocarbons and the following fractional selectivity for light hydrocarbons and the produced $CO_2$ though the WGS reaction were used [28]: $CH_4 = 0.05$, $C_2H_4 = 0.0005$, $C_2H_6 = 0.01$, $C_3H_6 = 0.02$, $C_3H_8 = 0.01$, $C_4H_8 = 0.02$, $C_4H_{10} = 0.01$ and $CO_2 = 0.01$. Stoichiometric amount of $H_2$ was fed to the hydrocracker. For the ATR the estimated optimum $H_2O$ and $O_2/C$ molar ratios were 0.6 and 0.2, respectively.

### 4.3. Methanol-based pathway

Table 5 presents the models parameters that are used for the reactors simulation. The adopted methodology for the methanol synthesis is based on the assumption of the chemical equilibrium. The methanol to olefins products yields were obtained from Avidan [46]. The oligomerization reaction process specifications for ethylene was adopted from Ref. [33], propylene from Ref. [35] and butane from Ref. [34]. Finally, for the hydrotreatment reactor process specifications it is assumed that all the olefins are converted into their respective n- and i-paraffins with a conversion rate of 90%.

**Table 4**
Reactors models specifications for the LTFT pathway.

| Reactor name | Reactor model | Process specifications | Associated reactions | Fractional conversion |
|---|---|---|---|---|
| Reverse Water Gas Shift | REQUIL | 900 °C/5 bar | $CO_2 + H_2 \rightarrow CO + H_2O$ $CO_2 + 4H_2 \rightarrow CH_4 + 2H_2O$ | – |
| Fischer-Tropsch | RSTOIC | 240 °C/35 bar $H_2/CO = 2$ | nCO + (2n+1)$H_2 \rightarrow C_nH_{2n+2} + nH_2O$ $CO + H_2O \rightarrow CO_2 + H_2$ | 0.85 (CO) |
| Hydrocracker | RSTOIC | 240 °C/35 bar | $C_{24}H_{30} + H_2 \rightarrow 2C_{12}H_{16}$ | 1 |
| | | | $C_{28}H_{58} + H_2 \rightarrow 2C_{14}H_{30}$ | 1 |
| | | | $C_{32}H_{66} + 3H_2 \rightarrow 4C_8H_{18}$ | 1 |
| | | | $C_{36}H_{74} + 3H_2 \rightarrow 4C_9H_{20}$ | 1 |
| | | | $C_{40}H_{82} + 3H_2 \rightarrow 4C_{10}H_{22}$ | 1 |
| | | | $C_{48}H_{98} + 3H_2 \rightarrow 4C_{12}H_{26}$ | 1 |
| | | | $C_{56}H_{114} + 3H_2 \rightarrow 4C_{14}H_{30}$ | 1 |
| | | | $C_{64}H_{130} + 3H_2 \rightarrow 4C_{16}H_{34}$ | 1 |
| Autothermal reactor | RGIBBS | 950 °C/5 bar $O_2/C = 0.6$ $H_2O/C = 0.2$ | – | – |

The distillation columns are modeled as RADFRAC. The Peng-Robinson property method with Boston-Mathias modification is selected with STEAMNBS as free water method.

**Table 5**
Reactors models specifications for the MeOH-based pathway.

| Reactor name | Reactor model | Process specifications | Associated reactions | Fractional conversion |
|---|---|---|---|---|
| Methanol synthesis | REQUIL | 250 °C/65 bar $H_2/CO_2 = 3.0$ | $CO + H_2O \rightarrow H_2 + CO_2$<br>$CO + 2H_2 \rightarrow CH_3OH$<br>$CO_2 + 3H_2 \rightarrow CH_3OH + H_2O$ | – |
| Methanol to Olefins | RSTOIC[a] | 450 °C/2 bar | $2CH_3OH \rightarrow DME + H_2O$<br>$DME \rightarrow C_2H_4 + H_2O$<br>$3DME \rightarrow 2C_2H_4 + 3H_2O$<br>$2C_2H_4 \rightarrow C_4H_8$<br>$C_2H_4 + C_3H_6 \rightarrow C_5H_{10}$<br>$2C_3H_6 \rightarrow C_6H_{12}$<br>$C_6H_{12} \rightarrow C_6H_6 + 3H_2$ | 1<br>0.637<br>1<br>0.077<br>0.008 ($C_2H_4$)<br>0.008<br>0.500 |
| Ethylene dimerization | RSTOIC | 25 °C/50 bar | $2C_2H_4 \rightarrow nC_4H_8$<br>$3C_2H_4 \rightarrow C_6H_{12}$<br>$2C_2H_4 \rightarrow iC_4H_8$ | 0.890<br>0.035<br>0.075 |
| Propylene oligomerization | RSTOIC | 270 °C/40 bar | $2C_3H_6 \rightarrow C_4H_8$<br>$3C_3H_6 \rightarrow C_9H_{18}$<br>$4C_3H_6 \rightarrow C_{12}H_{24}$<br>$5C_3H_6 \rightarrow C_{15}H_{30}$<br>$6C_3H_6 \rightarrow C_{18}H_{36}$ | 0.034<br>0.231<br>0.284<br>0.157<br>0.052 |
| Butene oligomerization | RSTOIC | 350 °C/10 bar | $2C_4H_8 \rightarrow C_8H_{16}$<br>$3C_4H_8 \rightarrow C_{12}H_{24}$<br>$4C_4H_8 \rightarrow C_{16}H_{32}$ | 0.394<br>0.344<br>0.041 |
| ATR | RGIBBS | 980 °C/150 bar<br>$O_2/C = 1.5$<br>$H_2O/C = 3.0$ | | |

All the distillation columns are modeled as RADFRAC. The Peng-Robinson property method is selected for all subsections apart from the methanol synthesis, where NRTL-RK is used.
[a] reactions occur in series.

### 4.4. Ethanol-based pathway

The methodology for the modeling of the ethanol production via DME is presented in detail elsewhere [47]. The only difference is that for the DME synthesis reaction model, a more simplified approach based on equilibrium is adopted (REQUIL). Table 6 presents the models parameters that are used for the reactors simulation.

The hydrotreatment model and the distillation columns modeling are based on the same approach to former case. The property method that is used for that model is ENRTL-RK.

## 5. Results and discussion

### 5.1. Material balance

The basic characteristics of the main streams of the four pathways are presented in the Supplementary Information. Table 7 presents the basic inlet/outlet streams flows and the respective indices as defined in Section 2.1. It is worth mention that all the examined cases have no direct $CO_2$ emissions as the initial amount of $CO_2$ is entirely transformed into synthetic fuel. The FT-based pathways show the best performance in terms of final products yield with LTFT pathway being superior as illustrated at the highest $Y_{e\text{-}jet}$ and $f_{e\text{-jet}}$ values as well. Moreover, the last one achieves the best utilization of the $H_2/CO_2$ feed gases. The MeOH based case has good performance indicators in terms of product yields and carbon utilization with slightly lower values that those of LTFT.

The $H_2/CO_2$ ratio for the ethanol-based case is the lowest, however this pathway results in the lowest kerosene yield. This is attributed to the relatively high selectivity in low carbon olefins after the oligomerization reaction process that cannot be used for synthetic kerosene formulation. The LTFT pathway has the lowest specific demands in oxygen for reforming owed to the reduced needs for light gas reforming compared

**Table 7**
Main flow rates and KPIs from mass balance calculations.

| | | CO2FT | LTFT | MeOH | EtOH |
|---|---|---|---|---|---|
| $CO_2$ flow in | kg/h | 4401 | 4401 | 4401 | 4401 |
| $H_2$ flow total | kg/h | 771 | 669 | 906 | 622 |
| Oxygen demand | kg/h | 1176 | 374 | 1514 | 0 |
| Steam demand for ATR | kg/h | 3783 | 105 | 1669 | 0 |
| Liquid products | kg/h | 1420 | 1420 | 1357 | 1355 |
| Jet Fuel flow | kg/h | 1073 | 1288 | 1165 | 885 |
| Wastewater flow | kg/h | 8711 | 4129 | 6284 | 3666 |
| CU | % | 75.7% | 90.7% | 82.7% | 62.4% |
| $Y_{e\text{-}jet}$ | % | 20.8% | 25.4% | 22.0% | 17.6% |
| $f_{e\text{-jet}}$ | % | 75.5% | 90.7% | 85.8% | 65.3% |

**Table 6**
Reactors models specifications for the ATJ section.

| Reactor name | Reactor model | Process specifications | Associated reactions | Fractional conversion |
|---|---|---|---|---|
| Guerbet reactor | RSTOIC | 150 °C/1.5 bar | $2Ethanol \rightarrow n\text{-}butanol + H_2O$<br>$3Ethanol \rightarrow hexanol + 2H_2O$<br>$3Ethanol \rightarrow 2ethyl\text{-}hexanol + 2H_2O$ | 0.271<br>0.026<br>0.009 |
| Alcohols dehydration | RSTOIC | 285 °C/1 bar | $Ethanol \rightarrow C_2H_4 + H_2O$<br>$Propanol \rightarrow C_3H_6 + H_2O$<br>$n\text{-}butanol \rightarrow 1\text{-}C_4H_8 + H_2O$<br>$2ethyl\text{-}hexanol \rightarrow C_6H_{12} + H_2O$<br>$Hexanol \rightarrow C_6H_{12} + H_2O$ | 1<br>1<br>0.8<br>1<br>1 |
| Hexene oligomerization | RSTOIC | 350 °C/10 bar | $2C_6H_{12} \rightarrow C_{12}H_{24}$ | |
| Butene oligomerization | RSTOIC | 350 °C/10 bar | $2\ 1\text{-}C_4H_8 \rightarrow C_8H_{16}$<br>$3\ 1\text{-}C_4H_8 \rightarrow C_{12}H_{24}$<br>$4\ 1\text{-}C_4H_8 \rightarrow C_{16}H_{32}$ | 0.2<br>0.7<br>0.1 |

to the other two cases. Supposing that the green hydrogen flow comes from a renewable driven electrolysis unit, the amount of oxygen that is co-produced is enough to cover the oxygen demands at the three cases where an ATR unit is considered. Special attention should be paid on the proper water management, as the wastewater is the largest stream of all at four cases. This effluent must be purified and reused either at the green hydrogen production unit or at the steam generation for ATR operation. This represents around 64% (MeOH case) to 81% (CO2FT case) of the total process water demands.

### 5.2. Energy balance

Table 8 summarizes all the aggregated main aspects of the heat and energy balance of the four pathways. The electrolyser consumption that is roughly calculated based on the assumption of a specific energy consumption of 53.79 kWh/$kg_{H2}$ [48] for a typical PEM electrolyser is included in the table results for comparison purpose but it is not taken into account at the overall calculations. Following the previous analysis on mass balance, LTFT demonstrates the best performance of all in terms of energy efficiency. More than 70% of fresh hydrogen energy content is finally converted into synthetic aviation fuel proving the effectiveness of this pathway.

An illustrative view of how the energy is distributed along each process is granted by the Sankey diagrams. The flows that represents the heat content of material streams are expressed on Higher Heating Value basis. In addition, the sensible heat of these streams has been taken into consideration in order to close the heat balance.

In Fig. 8, the important role of ATR is illustrated. The gas (reformate gas) that is produced from all the low-quality, low-importance gas from the oligomerization and hydrotreatment has slightly higher heat content of the fresh hydrogen that enters the FT synthesis reactor. Oligomerization and hydrotreatment are set to operate in high efficiency as the waste heat from these reactors is low. The waste heat from the ATR can be potentially exploited for the steam generation (this part has not been taken into detail in the CO2FT analysis).

Fig. 9 shows the Sankey diagram for the LTFT case. Although rWGS is an endothermic, energy demanding process, the required heat for its stable operation is 5.7% of the fresh hydrogen heat content. The ratio of the recycling streams to the fresh gas stream is the lowest of all the examined cases, this has beneficial impact on the reactors size and consequently to the total equipment cost. Thanks to the effective heat integration network, the waste heat from the overall process is 29% of the hydrogen heat input.

Fig. 10 depicts the impact of the ATR use for the light gas/purge gas utilization. A recycling stream of 19.8 MW with CO and $H_2$ is created and reused for methanol synthesis. As a result, this stream has a comparable heat content with that of hydrogen. The methanol to oligomers process chain has a very good energy conversion efficiency, as almost 10% of the heat content is lost as unexploited (waste) heat. Nevertheless, the paraffins that are final formed after the hydrotreatment process and their carbon number is $< 9$ and are not suitable for aviation fuel is greater than then final product streams (both jet fuel and diesel). This is attributed to the inevitable selectivity in light olefins at the oligomerization catalyst.

In the case of the EtOH route (Fig. 11), it is obvious that there is a considerable large amount of gas recycling between the DME and the Ethanol synthesis which is more than 5 times greater than the heat input of the hydrogen feed. The Sankey diagram indicates that a more efficient way to handle the CO/$H_2$ stream that is needed for DME carbonylation should be adopt in future improved versions of that pathway. As for upgrading part of ethanol into advanced paraffinic fuels, the energetic efficiency is 95.6% implying that the heat content of the inlet steams (ethanol and hydrogen) has a minor degradation during the 3-step ethanol conversion into jet fuel and diesel .

Table 9 summarizes the hot and cold utilities for the examined cases. CO2FT case has the lower hot utilities (only 0.11 MW HP steam) and a considerable amount of LP steam (10.6 MW) can be exploited externally or sold in the framework of industrial symbiosis. Similarly, at the LTFT case, 8.2 MW of LP steam is produced but 1.2 MW of heat with temperature >900 °C is required for the rWGS reactor operation. The MeOH case has practically no need for external heat as the amount of HP/IP/LP steam can be fulfilled from the IP/HP steam that is generated internally. The EtOH case has considerable amount of energy inflows and outflows at different forms (steam and refrigerants with multiple properties). All the cases apart from the last one have positive balance at inlet/outlet utilities, having thus an additional beneficial environmental impact by providing steam with zero carbon footprint.

Although a life cycle analysis is not considered in that study, it is easily extracted that the environmental impact of the produced synthetic kerosene and its potential GHG emissions reduction after replacement of fossil derived aviation fuel is mainly depended on the way that hydrogen is produced and the origin of the $CO_2$ stream. Moreover, the effective management of the utilities at the three first cases further decreases the carbon footprint at the produced synthetic fuels.

### 5.3. Exergy analysis

The results from the exergy analysis are presented in Table 10. CO2FT pathway is characterized from the high exergy that exits the process in the form of (waste) heat. The exergetic efficiency ($\eta_{ex}$) of LTFT pathway is the highest, verifying what has been previously mentioned in the energy analysis section. The high final products yield, the low exergy inlet because of the low power demand and relatively low heat input are the main factors for that. On the other hand, there is room for improvement in the performance of the alcohol-based pathways as it is illustrated from their high exergy loss. Especially for the ethanol-based pathway, new ways for producing DME more effectively or direct ethanol from $CO_2$ should be investigated. For the methanol-based pathway, the olefins oligomerization was based on certain studies that handle each light olefin separately. If their oligomerization can be accomplished as much as effectively even with the presence of the rest compounds after the MTO reactor, the refrigeration loads and the respective electricity consumption can be avoided at the MTO section for the light olefins separation.

### 5.4. Energy analysis of the LTFT pathway

As shown above, the LTFT pathway presents the best performance in terms of all indicators. In this paragraph, an energy analysis is presented by using the Aspen Energy Analyser. The results show that the current utility duty use is 29.88 MW and the target utility duty is 28.04 MW. These results demonstrate the efficient use of energy as energy savings potential is very low at 6.19%. The composite curves for $\Delta T_{min} = 10$ °C is shown in Fig. 12. The large amount of cold utility duty needed is due to the residual duty of the ATR (at 135 °C) and rWGS (at 150 °C) streams after the pre-heating of inlet streams of these two reactors and the steam generation required for ATR.

**Table 8**
Heat and Energy balance main results.

| | | CO2FT | LTFT | MeOH | EtOH |
|---|---|---|---|---|---|
| Thermal input $H_2$ (LHV base) | $MW_{th}$ | 25.67 | 22.29 | 30.20 | 20.70 |
| Electrolyser consumption | $MW_e$ | 41.12 | 35.70 | 48.37 | 33.17 |
| Compression Consumptions | $MW_e$ | 8.54 | 2.18 | 4.30 | 10.17 |
| Refrigeration demands | $MW_{th}$ | 0.00 | 0 | 0.21 | 7.822 |
| Power for refrigeration | $MW_e$ | 0 | 0 | 0.65 | 24.56 |
| Total power demands | $MW_e$ | 8.54 | 2.18 | 4.95 | 34.73 |
| External heat demands | $MW_{th}$ | 0.24 | 1.74 | 0 | 10.00 |
| Liquid fuels heat input (LHV) | $MW_{th}$ | 17.77 | 17.40 | 15.99 | 16.53 |
| Jet Fuel heat input (LHV) | $MW_{th}$ | 13.14 | 15.80 | 13.75 | 10.84 |
| EJFE | % | 51.2% | 70.9% | 45.5% | 52.4% |
| Total efficiency | % | 51.6% | 66.4% | 45.5% | 25.3% |

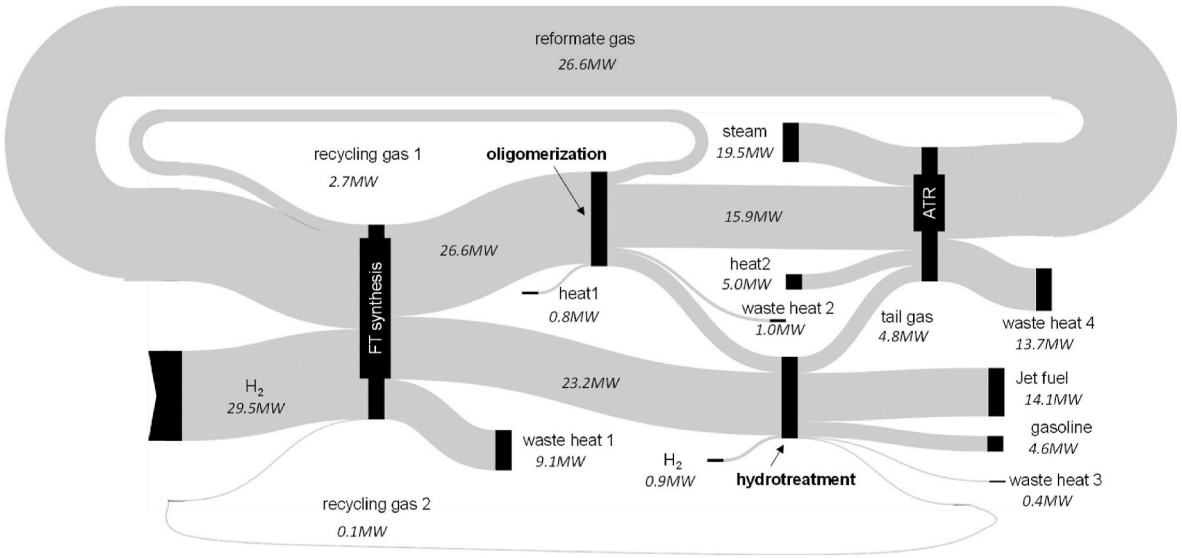


**Fig. 8.** Sankey diagram for CO2FT route (HHV basis).

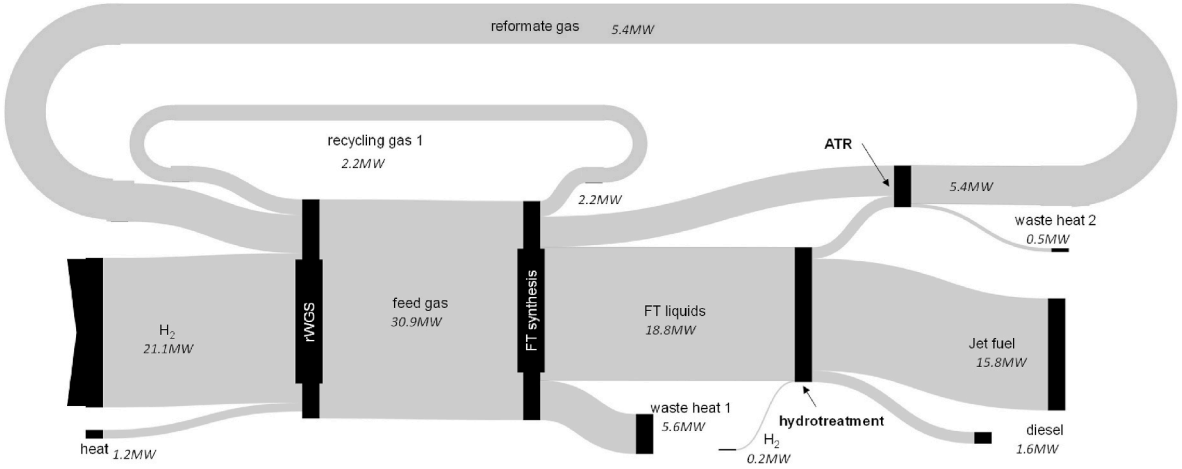


**Fig. 9.** Sankey diagram for LTFT route (HHV basis).

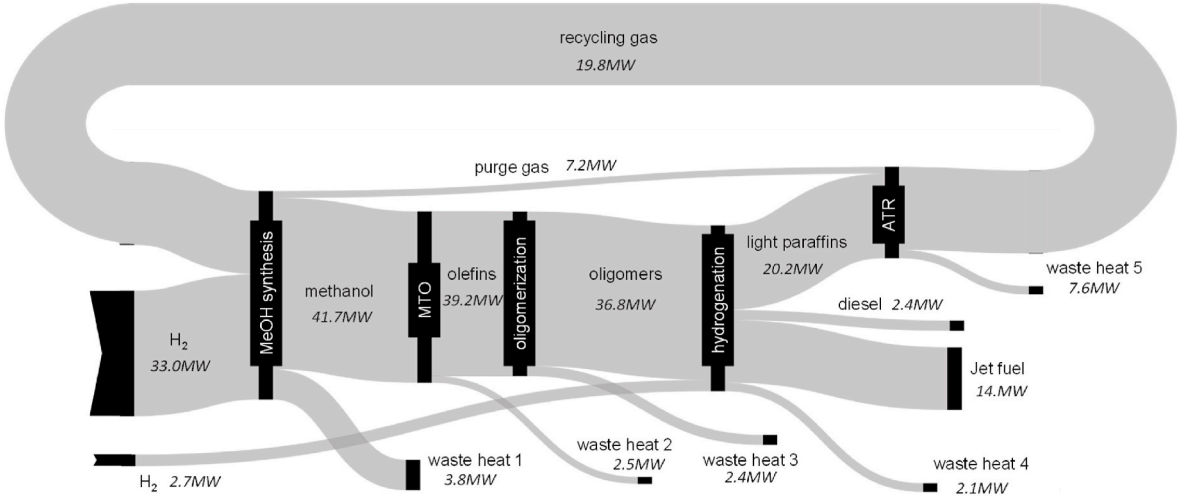


**Fig. 10.** Sankey diagram for methanol-based route (HHV basis).

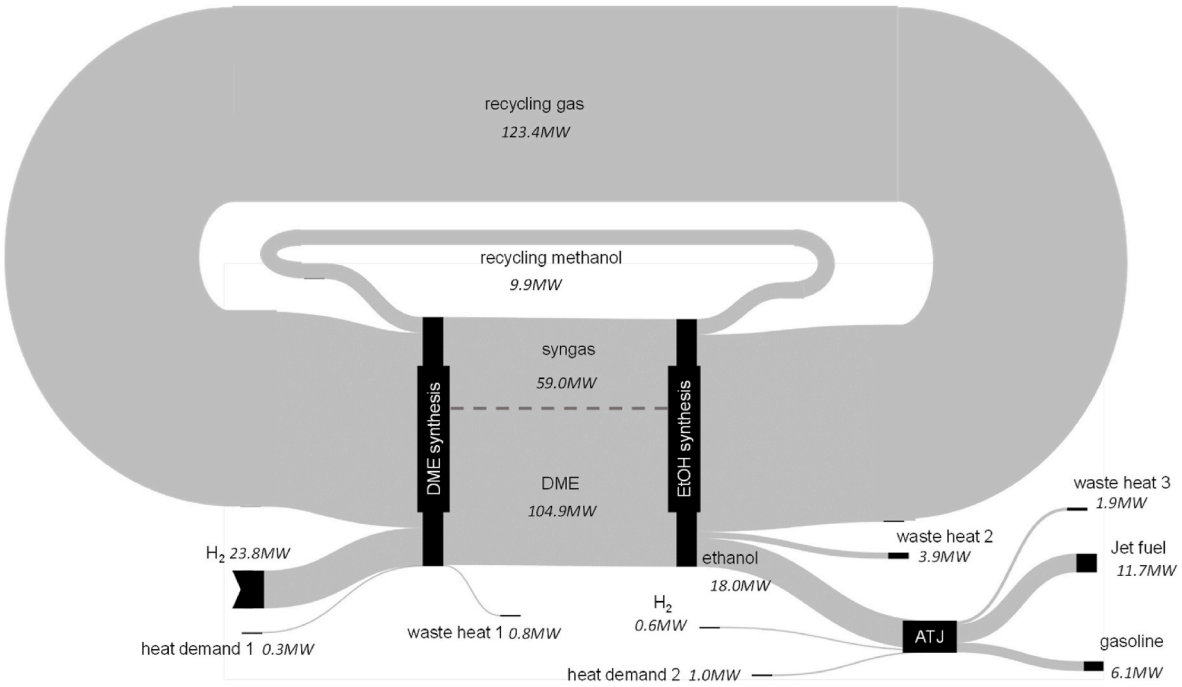


**Fig. 11.** Sankey diagram for ethanol-based route (HHV basis).

**Table 9**
Energy utilities (in kW) per each case.

| | CO2FT | LTFT | MeOH | EtOH |
|---|---|---|---|---|
| Very High T | | 1243 | | |
| Fired Heat | | | | 549 |
| HP Steam | 108 | 497 | 353 | 1007 |
| IP Steam | | | 23.8 | 1686 |
| LP Steam | 129 | | 1075 | 9209 |
| Air vent (heating) | | | 686 | |
| **Total Hot Utilities** | **237** | **1740** | **2138** | **12,451** |
| Cooling Water | 4945 | 2639 | 12,300 | 18,220 |
| Air vent (cooling) | | 577 | | |
| LP Steam Generation | 10,764 | 8164 | | 1333 |
| IP Steam Generation | | | 3564 | 318 |
| HP Steam Generation | | | 1305 | 239 |
| Refrigerant 1 | | | | 67 |
| Refrigerant 2 | | | 926 | 5456 |
| Refrigerant 3 | | | 166 | |
| **Total Cold Utilities** | **15,709** | **11,380** | **18,261** | **25,633** |

**Table 10**
Exergy balance results.

| Case | CO2FT | LTFT | MeOH | EtOH |
|---|---|---|---|---|
| $P_{in}$ (MW) | 8.54 | 2.18 | 4.95 | 34.73 |
| $\dot{E}_{H2,in}$ (MW) | 25.06 | 21.77 | 29.49 | 20.22 |
| $\dot{E}_{CO2,in}$ (MW) | 0.54 | 0.54 | 0.54 | 0.54 |
| $\dot{E}_{Q,in}$ (MW) | 3.81 | 1.09 | 0.00 | 2.12 |
| $\dot{E}_{in,tot}$ (MW) | 37.96 | 25.59 | 34.98 | 57.62 |
| $\dot{E}_{jet\ fuel}$ (MW) | 14.15 | 17.95 | 15.05 | 11.62 |
| $\dot{E}_{diesel\&gasoline}$ (MW) | 4.28 | 0.63 | 2.27 | 6.10 |
| $\dot{E}_{Q,out}$ (MW) | 10.89 | 3.90 | 2.91 | 4.24 |
| $\dot{E}_{out,tot}$ (MW) | 29.50 | 22.48 | 20.23 | 21.96 |
| $\dot{E}_{loss}$ (MW) | 8.65 | 3.11 | 14.76 | 35.66 |
| $\eta_{wasted}$ (%) | 28.7% | 15.2% | 8.3% | 7.4% |
| $\eta_{loss}$ (%) | 22.8% | 12.2% | 42.2% | 61.9% |
| $\eta_{ex}$ (%) | 48.5% | 72.6% | 49.5% | 30.8% |

### 5.5. Jet fuel characteristics

Some of the most critical properties of the final synthetic fuels that are calculated from Aspen Plus and are compared with the respective values from Jet-A1 specifications [49]. Table 11 summarizes these values. It is clear that the four pathways produce kerosene with basic properties close to the required Jet-A1 specifications. The deviations from the specifications are observed for density (in the range of 2.7–4.4%) and for 100% distillation for CO2FT (2.8%). Although the deviations are quite small, these can be eliminated if a better distillation of the kerosene fraction is configured by reducing a bit the lighter fractions that contribute to the decrease of density and the heavier fractions that favour the elevation of Distillation 100% temperature. Also, the addition of other compunds, e.g. aromatics, would result in better results for deisnty.

It should be underlined that even though it is not feasible to consider all the chemical compounds that exist in the final kerosene stream, the basic hydrocarbons that are considered in all cases can lead to a very good prediction at least of the basic jet fuel properties. This also is confirmed by other similar simulation studies that reported the respective jet fuel properties.

Finally, freezing point is of the most important property parameters for the evaluation of the e-kerosene product. However, Aspen does not support the calculation of the freezing point of mixtures and it is generally complicated to estimate the value using a prediction model. Indicatively, if a methodology based on the freezing point of each component found in the kerosene final stream and the respective volume fraction is applied for the four examined cases [50] the calculated freezing point values varies from −39.8 to −6.7 °C, which is above the maximum value for Jet A1 (−47 °C) and requires further investigation.

### 5.6. Comparison with other similar studies

The key performance indicators of the four pathways are compared with the respective results of indicative studies from the literature and summarized in Table 12. Apart from the main KPIs that are defined in Section 2.1, one more is added in order to express the conversion efficiency of all the produced fuels:

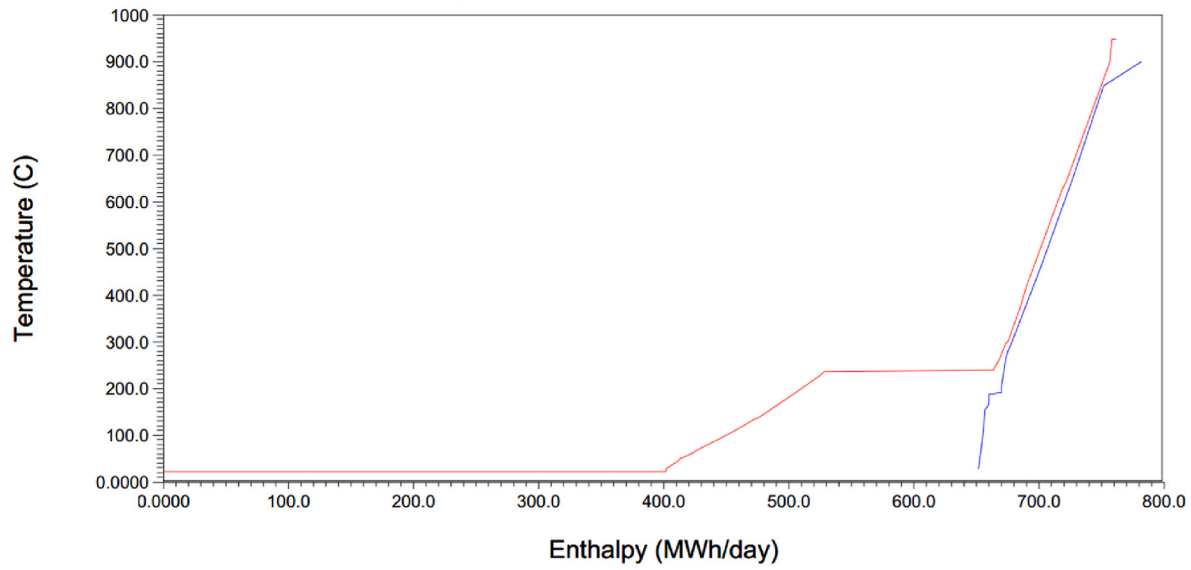


**Fig. 12.** Composite curve of the heat integrated LTFT flowsheet.

**Table 11**
Produced synthetic jet fuel properties.

| | | Jet A-1 | CO2FT | LTFT | MeOH | EtOH |
|---|---|---|---|---|---|---|
| **LHV** | MJ/kg | >42.80 | 44.12 | 44.15 | 42.50 | 44.10 |
| **Density** | kg/m$^3$ | 775–840 | 747.4 | 744.3 | 740.6 | 754.0 |
| **Viscosity (-20°C)** | mm$^2$/s | <8.0 | 4.32 | 5.28 | 3.36 | 5.44 |
| **Flash Point** | °C | >38 | 45.6 | 44.4 | 37.9 | 49.7 |
| **Distillation 10%** | °C | <205 | 163.6 | 153.1 | 156.1 | 171.45 |
| **Distillation 100%** | °C | <300 | 308.5 | 288.7 | 282.9 | 279.30 |

**Table 12**
KPIs from various synthetic fuels production systems and comparison.

| Study | technology | $Y_{e\text{-}jet}$ | $f_{e\text{-}jet}$ | *EJFE* | $\eta_{tot}$ | $\eta_{tot\ fuels}$ |
|---|---|---|---|---|---|---|
| König et al. [14] | rWGS - FT | 9.3% | 43.9% | 29.3% | 28.5% | 67.0% |
| Zang et al. [51] | rWGS - FT | 6.3% | 46.7% | 27.0% | 26.7% | 57.8% |
| Ruokonen et al. [13] | MeOH | 7.6% | 21.8% | 21.8% | 21.8% | 77.4% |
| this study | CO2FT | 20.8% | 75.5% | 51.2% | 51.6% | 69.2% |
| this study | LTFT | 25.4% | 90.7% | 70.9% | 66.4% | 78.1% |
| this study | MeOH | 22.0% | 85.8% | 45.5% | 45.5% | 52.9% |
| this study | EtOH | 17.6% | 65.3% | 52.4% | 25.3% | 79.9% |

$$\eta_{tot,fuels} = \frac{\sum \dot{m}_i \bullet LHV_i}{\dot{m}_{H2,in} \bullet LHV_{H2}} \quad \text{eq 33}$$

where $i$ = jet fuel, diesel, gasoline, gas fuel etc.

It makes clear that the four pathways investigated in this study present a significant advancement in maximization of jet fuel production yield, as illustrated from the $Y_{e\text{-}jet}$ and $f_{e\text{-}jet}$ that are higher than the respective performance values found in the literature. Moreover, the way that the inlet energy (hydrogen heat input, heat and electricity) are converted into the desired synthetic aviation fuel is more efficient. The EtOH based route presents the highest performance in terms of hydrogen conversion into all the liquid fuels, even though the e-kerosene yield ($Y_{e\text{-}jet}$) is the lowest of the four new processes but not lower that the two studies from the literature.

## 6. Conclusions

This study presents two Fischer-Tropsch based (one unconventional high temperature FT without a reverse WGS reactor in addition to a conventional LTFT process) and two new (light alcohols based) pathways for $CO_2$ catalytic conversion into synthetic jet fuel. They were developed in such way that the jet fuel fraction is maximized compared to other liquid fuels fraction (gasoline and diesel) and the main properties to follow the respective Jet-A1 specifications. The analysis of these pathways was on the basis of the process design and comparative assessment was made in terms of process performance, energy and exergy. The process simulations results revealed that LTFT pathway presents the best performance as it is illustrated from the highest values of jet fuel yields and the energy & exergy indices. This implies that the most efficient way to produce synthetic kerosene from $CO_2$ with thermocatalytic techniques is first to convert it into CO and then the $CO/H_2$ stream to be transformed into hydrocarbons via Fischer-Tropsch synthesis. The alcohol-based routes presented also good performance in terms of the target product yield and the respective carbon utilization and have the potential to be competitive to the FT-based pathways if certain improvements in catalysts performance (higher selectivity in $C_{12}$–$C_{14}$ compounds) is achieved. All the proposed pathways demonstrated improved performance compared to other similar approaches in the literature as concerns the maximization of the aviation fuel fraction, when it is considered as the desired end-product. However, a weakness is the higher level of complexity for that cases as a certain number of catalytic reactors and recovery units of the intermediate products are required in order to convert methanol and ethanol into long chain paraffinic fuels. An overall assessment in terms of production cost and environmental impact is needed as a future work in order to get a clear insight of the examined pathways prospects. Such a holistic analysis will address to determine the proper plant capacity and the influence of the C utilization unit on the total investment compared to the rest parts of the system i.e. the hydrogen and pure $CO_2$ production units.

## Author contribution

K. Atsonios: Conceptualization, Methodology, Investigation, Software, Validation, Visualization, Writing – original draft, J. Li: Software, Validation, V.J. Inglezakis: Project administration, Conceptualization, Methodology, Validation, Software, Writing – review & editing.

## Declaration of competing interest

The authors declare that they have no known competing financial interests or personal relationships that could have appeared to influence

the work reported in this paper.

## Data availability

No data was used for the research described in the article.

## Abbreviations

| | |
|---|---|
| ASF | Anderson-Schulz-Flory |
| ATJ | Alcohol to Jet |
| ATR | autothermal reactor |
| CHJ | catalytic hydrothermolysis |
| COP | coefficient of performance |
| CO2FT | High-temperature Fischer-Tropsch synthesis without rWGS |
| CU | Carbon Utilization |
| DME | dimethyl ether |
| EA | ethyl acetate |
| EJFE | Energetic Jet Fuel Efficiency |
| EtOH | ethanol |
| FT | Fischer-Tropsch |
| FT-SKA | Fischer-Tropsch synthetic kerosene with aromatics |
| FT-SRK | Fischer-Tropsch synthetic paraffinic kerosene |
| GHG | greenhouse gas |
| HC-HEFA-SPK | synthesized paraffinic kerosene from hydrocarbon-hydroprocessed esters & fatty acids |
| HEFA | Hydroprocessed Esters and Fatty Acids |
| HHV | Higher Heating Value |
| IP | Intermediate pressure |
| HP | High pressure |
| LHV | Lower Heating Value |
| LP | Low pressure |
| LTFT | Low Temperature Fischer-Tropsch |
| MA | methyl acetate |
| MeOH | methanol |
| MOGD | Mobil's olefins to gasoline and distillate |
| MTO | methanol-to-olefins |
| PEM | Proton Exchange Membrane |
| rWGS | reverse water gas shift reaction |
| SAF | sustainable aviation fuel |
| SIP | synthesized iso-paraffins |
| WGS | water-gas shift reaction |

## Appendix B. Supplementary data

Supplementary data to this article can be found online at https://doi.org/10.1016/j.energy.2023.127868.

## References


[1] Kyriakopoulos GL, Streimikiene D, Baležentis T. Addressing challenges of low-carbon energy transition. Energies 2022;15. https://doi.org/10.3390/en15155718.

[2] EEA. Greenhouse gas emissions by aggregated sector n.d. https://www.eea.europa.eu/data-and-maps/daviz/ghg-emissions-by-aggregated-sector-5#tab-dashboard-02.

[3] Eurostat. Greenhouse gas emissions falling in most source sectors n.d. https://ec.europa.eu/eurostat/en/web/products-eurostat-news/-/ddn-20220823-1.

[4] Woodroffe JD, Harvey BG. High-performance, biobased, jet fuel blends containing hydrogenated monoterpenes and synthetic paraffinic kerosenes. Energy Fuel 2020;34:5929–37. https://doi.org/10.1021/acs.energyfuels.0c00274.

[5] Wang M, Dewil R, Maniatis K, Wheeldon J, Tan T, Baeyens J, et al. Biomass-derived aviation fuels: challenges and perspective. Prog Energy Combust Sci 2019;74:31–49. https://doi.org/10.1016/J.PECS.2019.04.004.

[6] Zhang L, Dang Y, Zhou X, Gao P, Petrus van Bavel A, Wang H, et al. Direct conversion of $CO_2$ to a jet fuel over CoFe alloy catalysts. Innovation 2021;2. https://doi.org/10.1016/j.xinn.2021.100170.

[7] Marchese M, Giglio E, Santarelli M, Lanzini A. Energy performance of Power-to-Liquid applications integrating biogas upgrading, reverse water gas shift, solid oxide electrolysis and Fischer-Tropsch technologies. Energy Convers Manag X 2020;6:100041. https://doi.org/10.1016/J.ECMX.2020.100041.

[8] Pratschner S, Hammerschmid M, Müller FJ, Müller S, Winter F. Simulation of a pilot scale power-to-liquid plant producing synthetic fuel and wax by combining fischer–tropsch synthesis and SOEC. Energies 2022;15:4134. https://doi.org/10.3390/en15114134.

[9] INERATEC. Sustainable e-fuels for aviation n.d. https://ineratec.de/en/e-fuels-for-aviation/. [Accessed 14 November 2022].

[10] ExxonMobil. ExxonMobil methanol to jet technology to provide new route for sustainable aviation fuel production n.d. https://www.exxonmobilchemical.com/en/resources/library/library-detail/101116/exxonmobil_sustainable_aviation_fuel_production_en?utm_source=google&utm_medium=cpc&utm_campaign=cl_downstream_none&ds_k=&gclsrc=aw.ds&&ppc_keyword=aviation fuel&gclid=CjwKCAjwo.

[11] Sudiro M, Bertucco A. Production of synthetic gasoline and diesel fuel by alternative processes using natural gas and coal: process simulation and optimization. Energy 2009;34:2206–14. https://doi.org/10.1016/j.energy.2008.12.009.

[12] Navas-Anguita Z, Cruz PL, Martín-Gamboa M, Iribarren D, Dufour J. Simulation and life cycle assessment of synthetic fuels produced via biogas dry reforming and Fischer-Tropsch synthesis. Fuel 2019;235:1492–500. https://doi.org/10.1016/j.fuel.2018.08.147.

[13] Ruokonen J, Nieminen H, Dahiru AR, Laari A, Koiranen T, Laaksonen P, et al. Modelling and cost estimation for conversion of green methanol to renewable liquid transport fuels via olefin oligomerisation. Processes 2021;9. https://doi.org/10.3390/pr9061046.

[14] König DH, Baucks N, Dietrich RU, Wörner A. Simulation and evaluation of a process concept for the generation of synthetic fuel from CO2 and H2. Energy 2015;91:833–41. https://doi.org/10.1016/j.energy.2015.08.099.

[15] Petersen AM, Chireshe F, Okoro O, Gorgens J, van Dyk J. Evaluating refinery configurations for deriving sustainable aviation fuel from ethanol or syncrude. Fuel Process Technol 2021;219. https://doi.org/10.1016/j.fuproc.2021.106879.

[16] Atsonios K, Kougioumtzis M-A, Panopoulos KD, Kakaras E. Alternative thermochemical routes for aviation biofuels via alcohols synthesis: process modeling, techno-economic assessment and comparison. Appl Energy 2015;138. https://doi.org/10.1016/j.apenergy.2014.10.056.

[17] De Falco M, Natrella G, Capocelli M, Popielak P, Sołtysik M, Wawrzyńczak D, et al. Exergetic analysis of DME synthesis from CO2 and renewable hydrogen. Energies 2022;15. https://doi.org/10.3390/en15103516.

[18] Szargut J. Exergy method: technical and ecological applications. 2005. UK.

[19] Kotas TJ. The exergy method of thermal plant analysis. Butterworth-Heinemann; 1985. https://doi.org/10.1016/C2013-0-00894-8.

[20] Wang W, Wang S, Ma X, Gong J. Recent advances in catalytic hydrogenation of carbon dioxide. Chem Soc Rev 2011;40:3703–27. https://doi.org/10.1039/c1cs15008a.

[21] Choi YH, Jang YJ, Park H, Kim WY, Lee YH, Choi SH, et al. Carbon dioxide Fischer-Tropsch synthesis: a new path to carbon-neutral fuels. Appl Catal, B 2017;202:605–10. https://doi.org/10.1016/j.apcatb.2016.09.072.

[22] Rodemerck U, Holeňa M, Wagner E, Smejkal Q, Barkschat A, Baerns M. Catalyst development for CO2 hydrogenation to fuels. ChemCatChem 2013;5:1948. https://doi.org/10.1002/cctc.201200879. –55.

[23] Jiang F, Liu B, Geng S, Xu Y, Liu X. Hydrogenation of CO2 into hydrocarbons: enhanced catalytic activity over Fe-based Fischer-Tropsch catalysts. Catal Sci Technol 2018;8:4097–107. https://doi.org/10.1039/c8cy00850g.

[24] de Klerk A. Fischer-tropsch refining. PhD. Univeristy of Pretoria; 2008.

[25] Steynberg A, Dry M. Fischer-tropsch technology. Elsevier; 2004.

[26] Chen X, Chen Y, Song C, Ji P, Wang N, Wang W, et al. Recent advances in supported metal catalysts and oxide catalysts for the reverse water-gas shift reaction. Front Chem 2020;8. https://doi.org/10.3389/fchem.2020.00709.

[27] Adams TA, Barton PI. Combining coal gasification and natural gas reforming for efficient polygeneration. Fuel Process Technol 2011;92:639–55. https://doi.org/10.1016/j.fuproc.2010.11.023.

[28] Scott AJ, Adams II TA. Biomass-gas-and-nuclear-to-liquids (BGNTL) processes Part I: model development and simulation. Can J Chem Eng 2018;96:1853–71.

[29] Link F, Ahad N, de Klerk A. Low-pressure hydrocracking of wax over Pt/SiO2-Al2O3to produce kerosene for synthetic jet fuel. ACS (Am Chem Soc) Symp Ser 2021;1379:311–52. https://doi.org/10.1021/bk-2021-1379.ch012. American Chemical Society.

[30] Zhang Y, Dou B, Liu X, Fan H, Geng C, Liu X, et al. Experimental and theoretical study of the adsorption of mixed low carbon alcohols and acids from Fischer Tropsch synthesis wastewater by activated carbon. Fuel 2023;339:126928. https://doi.org/10.1016/j.fuel.2022.126928.

[31] Zhang R, Huang Y, Zheng K, Xu C. Design and control of fraction cutting for the separation of mixed alcohols from the Fischer–Tropsch aqueous by-products. Chin J Chem Eng 2022;50:143–54. https://doi.org/10.1016/j.cjche.2022.08.005.

[32] Gogate MR. Methanol-to-olefins process technology: current status and future prospects. Petrol Sci Technol 2019;37:559–65. https://doi.org/10.1080/10916466.2018.1555589.

[33] Metzger ED, Brozek CK, Comito RJ, Dincă M. Selective dimerization of ethylene to 1-butene with a porous catalyst. ACS Cent Sci 2016;2:148–53. https://doi.org/10.1021/acscentsci.6b00012.

[34] Zhang X, Zhong J, Wang J, Gao J, Liu A. Trimerization of butene over Ni-doped zeolite catalyst: effect of textural and acidic properties. Catal Lett 2008;126:388–95. https://doi.org/10.1007/s10562-008-9642-y.

[35] Li X, Han D, Wang H, Liu G, Wang B, Li Z, et al. Propene oligomerization to high-quality liquid fuels over Ni/HZSM-5. Fuel 2015;144:9–14. https://doi.org/10.1016/J.FUEL.2014.12.005.

[36] Lu WZ, Teng LH, Xiao W De. Simulation and experiment study of dimethyl ether synthesis from syngas in a fluidized-bed reactor. Chem Eng Sci 2004;59:5455–64. https://doi.org/10.1016/J.CES.2004.07.031.
[37] Lu P, Yang G, Tanaka Y, Tsubaki N. Ethanol direct synthesis from dimethyl ether and syngas on the combination of noble metal impregnated zeolite with Cu/ZnO catalyst. Catal Today 2014;232:22–6. https://doi.org/10.1016/J.CATTOD.2013.10.042.
[38] Atsonios K, Panopoulos KD, Kakaras E. Thermocatalytic CO2 hydrogenation for methanol and ethanol production: process improvements. Int J Hydrogen Energy 2016;41:792–806. https://doi.org/10.1016/J.IJHYDENE.2015.12.001.
[39] Wang Y, Wang K, Zhang B, Peng X, Gao X, Yang G, et al. Direct conversion of CO2 to ethanol boosted by intimacy-sensitive multifunctional catalysts. ACS Catal 2021;11:11742–53. https://doi.org/10.1021/acscatal.1c01504.
[40] Geleynse S, Brandt K, Garcia-Perez M, Wolcott M, Zhang X. The alcohol-to-jet conversion pathway for drop-in biofuels: techno-economic evaluation. ChemSusChem 2018;11:3728–41. https://doi.org/10.1002/cssc.201801690.
[41] Dowson GRM, Haddow MF, Lee J, Wingad RL, Wass DF. Catalytic conversion of ethanol into an advanced biofuel: unprecedented selectivity for n-butanol. Angew Chem Int Ed 2013;52:9005. https://doi.org/10.1002/anie.201303723. 8.
[42] Saeidi S, Amin NAS, Rahimpour MR. Hydrogenation of CO2 to value-added products - a review and potential future developments. J CO2 Util 2014;5:66–81. https://doi.org/10.1016/j.jcou.2013.12.005.
[43] Landau Mv, Vidruk R, Herskowitz M. Sustainable production of green feed from carbon dioxide and hydrogen. ChemSusChem 2014;7:785–94. https://doi.org/10.1002/cssc.201301181.
[44] Fazeli H, Panahi M, Rafiee A. Investigating the potential of carbon dioxide utilization in a gas-to-liquids process with iron-based Fischer-Tropsch catalyst. J Nat Gas Sci Eng 2018;52:549–58. https://doi.org/10.1016/j.jngse.2018.02.005.
[45] Meurer A, Kern J. Fischer–tropsch synthesis as the key for decentralized sustainable kerosene production. Energies 2021;14. https://doi.org/10.3390/en14071836.
[46] Avidan AA. Gasoline and distillate fuels from methanol. Stud Surf Sci Catal 1988;36:307–23. https://doi.org/10.1016/S0167-2991(09)60524-3.
[47] Atsonios K, Panopoulos KD, Kakaras E. Thermocatalytic $CO_2$ hydrogenation for methanol and ethanol production: process improvements. Int J Hydrogen Energy 2016;41. https://doi.org/10.1016/j.ijhydene.2015.12.001.
[48] Tenhumberg N, Büker K. Ecological and economic evaluation of hydrogen production by different water electrolysis technologies. Chem Ing Tech 2020;92:1586–95. https://doi.org/10.1002/cite.202000090.
[49] Standard, Alternative Fuel Specifications. Biofuels for aviation: feedstocks, technology and implementation. 2016. p. 351–7. https://doi.org/10.1016/B978-0-12-804568-8.00023-8.
[50] Boehm RC, Coburn AA, Yang Z, Wanstall CT, Heyne JS. Blend prediction model for the freeze point of jet fuel range hydrocarbons. Energy Fuels 2022;36:12046–53. https://doi.org/10.1021/acs.energyfuels.2c02063.
[51] Zang G, Sun P, Elgowainy AA, Bafana A, Wang M. Performance and cost analysis of liquid fuel production from H2and CO2based on the Fischer-Tropsch process. J CO2 Util 2021;46. https://doi.org/10.1016/j.jcou.2021.101459.